RSC Advances

ROYAL SOCIETY OF CHEMISTRY

REVIEW

View Article Online
View Journal | View Issue

Check for updates

Cite this: *RSC Adv.*, 2021, **11**, 11918

Surface modification and functionalization of powder materials by atomic layer deposition: a review

Yiyun Hu,[ab] Jian Lu[c] and Hao Feng*[abc]

Powder materials are a class of industrial materials with many important applications. In some circumstances, surface modification and functionalization of these materials are essential for achieving or enhancing their expected performances. However, effective and precise surface modification of powder materials remains a challenge due to a series of problems such as high surface area, diffusion limitation, and particle agglomeration. Atomic layer deposition (ALD) is a cutting-edge thin film coating technology traditionally used in the semiconductor industry. ALD enables layer by layer thin film growth by alternating saturated surface reactions between the gaseous precursors and the substrate. The self-limiting nature of ALD surface reaction offers angstrom level thickness control as well as exceptional film conformality on complex structures. With these advantages, ALD has become a powerful tool to effectively fabricate powder materials for applications in many areas other than microelectronics. This review focuses on the unique capability of ALD in surface engineering of powder materials, including recent advances in the design of ALD reactors for powder fabrication, and applications of ALD in areas such as stabilization of particles, catalysts, energetic materials, batteries, wave absorbing materials and medicine. We intend to show the versatility and efficacy of ALD in fabricating various kinds of powder materials, and help the readers gain insights into the principles, methods, and unique effects of powder fabrication by ALD.

Received 14th January 2021
Accepted 5th March 2021

DOI: 10.1039/d1ra00326g

rsc.li/rsc-advances

1. Introduction

Powder materials are widely used in various industrial areas. In many circumstances, surface modification and functionalization of powder materials are essential for achieving or enhancing the desired performances. Effective and precise surface modification of powder materials has been an everlasting topic for both academia and industry. In order to introduce the desired physical

---

[a] *Science and Technology on Combustion and Explosion Laboratory, Xi'an Modern Chemistry Research Institute, 168 E. Zhangba Road, Xi'an, 710065, Shanxi, PR China. E-mail: fenghao98@hotmail.com*
[b] *Laboratory of Material Surface Engineering and Nanofabrication, Xi'an Modern Chemistry Research Institute, 168 E. Zhangba Road, Xi'an, 710065, Shanxi, PR China*
[c] *State Key Laboratory of Fluorine and Nitrogen Chemicals, Xi'an Modern Chemistry Research Institute, 168 E. Zhangba Road, Xi'an, 710065, Shanxi, PR China*

Yiyun Hu received the bachelor degree in Material Science and Engineering from Tsinghua University in 2018. She is currently working towards the master degree in Material Science under the supervision of Prof. Hao Feng at Xi'an Modern Chemistry Research Institute. Her current research project is about fabrication of nano energetic materials by atomic layer deposition.

Prof. Jian Lu is currently the director of State Key Laboratory of Fluorine & Nitrogen Chemicals at Xi'an Modern Chemistry Research Institute. He received the PhD degree from Shanxi Institute of Coal Chemistry, Chinese Academy of Science in 1998. His research interest focuses on catalytic technologies for the green synthesis of fluorine-containing chemicals.

or chemical properties to the powder, many methods, such as sol–gel processing and chemical vapor deposition (CVD), have been developed, to produce functional thin films or discontinuous structures on the surfaces of the prime particles. Although these methods have been successfully applied to many powder systems, most of these methods fail to achieve precise control over the thickness of the surface fabrication layer, which may result in compromised effects and poor consistency or reproducibility. In addition, uncontrolled film thickness may easily cause permanent aggregation of primary particles, which can be detrimental to the performance of the powder.[1]

Unlike many other vapor-phase deposition techniques, atomic layer deposition (ALD) is not a line-of-sight dependent process. ALD processes are based on cyclical self-limiting chemisorptions taking place on the surface of the substrate. In a typical ALD process as depicted in Fig. 1, two precursors are alternately introduced in the vapor form, and each reacts with the surface functional groups generated during the previous reaction step. Each step of the surface reaction is self-limiting and the two reaction steps are separated by inert gas purges which remove the unreacted precursors and reaction by-products. Thus the film thickness is precisely controlled by the number of ALD cycle performed. The typical ALD film growth rate for most inorganic materials is ranged between 0.01 to 0.25 nm per cycle, depending on the specific type of material, precursors, and reaction conditions.[2]

The special film growth mechanism endows ALD the unique capability of producing conformal coatings on materials with complex structures. A powder bed can be considered a porous system with many inter-connected channels and crevices. In an ALD process, when the gaseous precursor is introduced it can infiltrate the channels and crevices. The self-limiting reactions take place only on the surface and the gas phase over-reactions are avoided. Therefore, continuous exposure to the gaseous precursor until the surface reactions become saturated is the key to obtaining complete and uniform coating on powder materials. This can be achieved by developing advanced ALD reactor and precursor supply systems. Detailed discussions on this topic will be carried out in the next section.

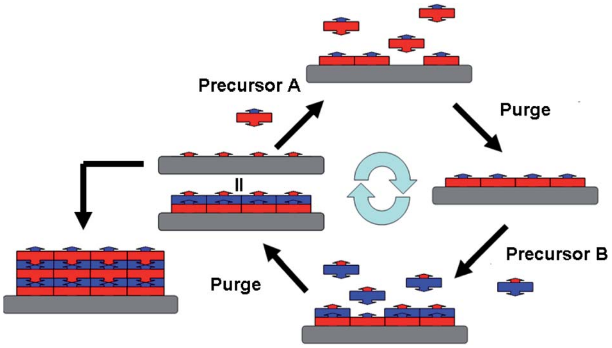

Fig. 1 Schematic picture of a typical ALD process.

Prof. Hao Feng is the leader of Laboratory of Material Surface Engineering and Nano Fabrication at Xi'an Modern Chemistry Research Institute. He received the PhD degree from Northwestern University, IL, USA in 2007. His research interest focuses on the applications of atomic layer deposition in catalysis, energetic materials, and functional thin films.

A large number of materials can be made by ALD, including many inorganic materials, a variety of organic polymers, and hybrid materials prepared by alternating inorganic and organic blocks.[3] Most types of powder materials, including micrometer or nanometer scale inorganic or organic particles, can be effectively coated. With ALD the structure of the surface fabrication layer can be controlled at atomic level precision, and the surface properties can be precisely tuned. By introducing desired physical or chemical properties to the surface, ALD can provide unlimited possibilities to the design and synthesis of novel functional materials.

This review is intended for introducing recent advances in powder material fabrication by ALD, including reactor and process design for powder fabrication, and applications in many different areas such as stabilization of particles, catalysts, energetic materials, batteries, wave absorbing materials, and medicine. We hope to show the versatility and efficacy of ALD in fabricating various kind of powder materials, and help the readers gain insights into the principles, methods, and effects of powder fabrication by ALD. Some existing reviews on related topics are recommended for a more comprehensive understanding on ALD.[1–7]

2. ALD reactor and process for powder fabrication

It is generally accepted that ALD was pioneered in Finland in the early 1970s by Suntola and Jorma under the name of "atomic layer epitaxy" (ALE).[8] In 2000 Ferguson *et al.* demonstrated that ALD technique could be used to coat ultrathin films onto the surfaces of primary particles.[9] Since then, the great interest in functionalized particles has been driving researchers to develop economically scalable and easy-to-operate ALD reactors for powder fabrication.

Currently, powder or particle ALD is mainly carried out in fixed bed, agitated bed, or fluidized bed reactors. Fixed bed ALD reactors are only suitable for processing small amounts of powder samples. When a large amount of powder is loaded, it is difficult for the gas phase precursor to diffuse into the bottom/inside of the powder bed in each precursor injection step, so that saturation of the surface reaction cannot be guaranteed, resulting in nonuniform coating, or more frequently, coating only on the top or external layer of the powder bed. Libera *et al.* reported an example of depositing ZnO on high surface area silica gel particles using a fixed bed ALD reactor.[10] The silica gel powder was held in a container covered by a fine stainless mesh as shown in Fig. 2a. The gap between the powder layer and the

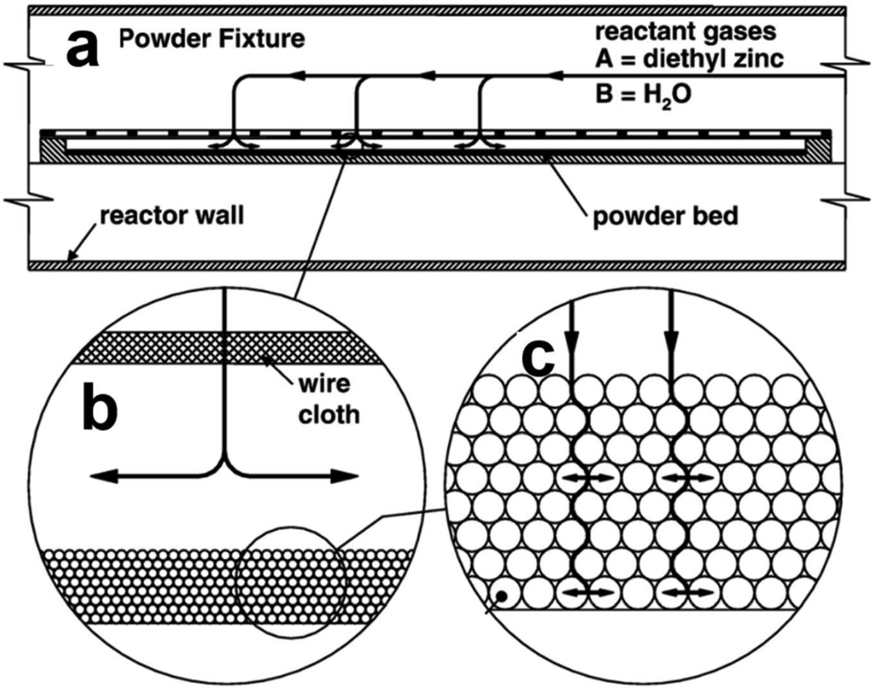

Fig. 2 (a) Cross-sectional schematic picture of the powder coating fixture of a fixed bed ALD reactor; detailed structures of the cover (b) and the powder bed (c). Reprinted with permission from ref. 10, Copyright (2008), Elsevier.

cover as well as the thickness of the powder layer should be carefully controlled (Fig. 2b and c) to ensure rapid diffusion of gases between particles. A thick powder bed may lead to non-uniform ZnO coating between particles or inside the particles. Therefore, when using a fixed-bed reactor for powder ALD, it is very important to control the amount of substrate material, uniformly spread the powder in the flow path, and provide sufficient ALD sequence time to ensure the saturated surface reaction. Nevertheless, when large-scale production is needed, the limitations of fixed-bed reactors are difficult to avoid, and other reactor designs must be applied.

Since the introduction of fluidized bed reactors (FBRs) to ALD, a variety of materials have been deposited on different types of powders using FBRs.[11–13] Some of the fluidized bed ALD reactors utilize vibration, stirring or other methods of agitation to prevent particles from agglomerating during the coating process, and thus improve the uniformity of coatings. King *et al.* reported a FBR with mechanical vibration and agitation (Fig. 3a).[14] In this reactor inert carrier gas purge was combined with mechanical stirring to effectively fluidize nanometer or micrometer-sized particles. During the fluidization process, agglomerated particles showed a dynamic agglomeration

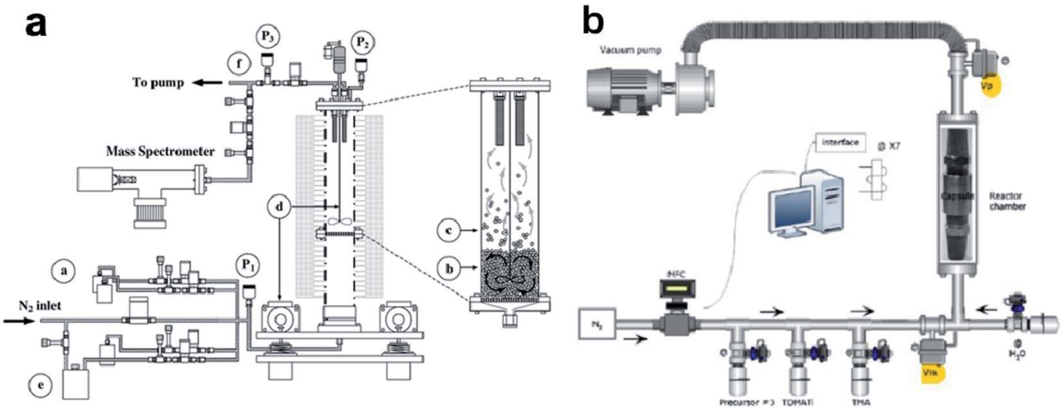

Fig. 3 Configurations of ALD reactors for powder fabrication: (a), schematic of the fluidized bed ALD reactor. The flexibility of the dosing zone a) allows for the controlled delivery of a variety of precursors. The particle bed b) is fluidized using either the inert purge gas or the reactive precursor itself. Particles entering the splash zone c) fluidize as soft agglomerates, and operating velocities are controlled to minimize particle elutriation to the filters. Mechanical bed agitation d) facilitates fluidization and precursor bubblers e) can be used to maintain fluidization during dosing. Real-time gas sampling occurs at the outlet of the reactor f) using *in situ* mass spectrometry. Three capacitance manometers (P1, P2, P3) are employed to monitor fluidization and proper system operation. Reprinted with permission from ref. 14, Copyright (2007), Elsevier. (b) Schematic of the pulsed-bed ALD system. Reprinted with permission from ref. 18, Copyright (2014), Elsevier.

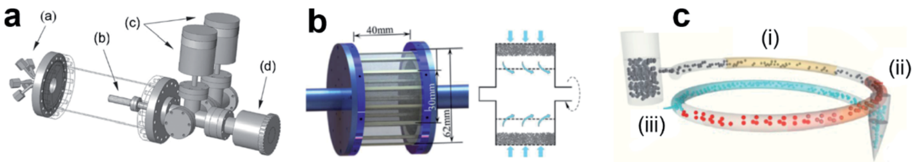

Fig. 4 (a) Schematic diagram of the rotary ALD reactor, showing a), multiple input dosing flange, b), small porous metal cylinder, c), 10 and 1000 Torr capacitance manometers, and d), magnetically coupled rotary manipulator. Reprinted with permission from ref. 19. Copyright (2007), American Vacuum Society. (b) Simplified assembly drawing of the rotating fluidized bed ALD reactor and schematic diagram of the particle cartridge. Reprinted with permission from ref. 20. Copyright (2015), with the permission of AIP Publishing. (c) Pneumatic transport line in the spatial ALD reactor made of three segments: preheating zone (i), precursor reaction zone (ii), co-reactant reaction zone (iii), and a collection vessel. Reprinted with permission from ref. 23. Copyright (2015), American Vacuum Society.

behavior, which means the primary particles will be torn away from some agglomerates and then be absorbed by other agglomerates. In other words, the agglomerates of primary particles continuously break apart and form again. With such mechanism, the surfaces of all primary particles will be exposed to ALD precursors and be uniformly coated.[15]

Powder ALD in FBRs can be operated either at reduced pressure or at atmospheric pressure. Beetstra *et al.* demonstrated that ALD of Al_2O_3 on $LiMn_2O_4$ powder (200–500 nm) is feasible using a fluidized bed reactor under atmospheric pressure.[16] One hundred grams of the $LiMn_2O_4$ powder was loaded in the FBR and the primary particles were coated individually. Some of the gaps between particles were filled with Al_2O_3, which might be caused by water build-up due to insufficient inert gas purge. In another case, Pd nanoparticles were deposited onto graphene (GE) nanoplatelets using a FBR at atmospheric pressure.[17] The Pd/GE obtained by atmospheric pressure ALD showed lower impurity content, better dispersion and more uniform distribution of Pd nanoparticles. Obviously, it will be much more convenient to scale-up the ALD process under atmospheric pressure, however, efficient supplying and removing of precursors and avoiding side reactions are still challenging under atmospheric pressure.

Despite their efficacy for coating primary particles, FBRs face the problem of low precursor utilization efficiency, because a large fraction of the precursor may be carried away by the fast, continuous gas flow necessary for particle fluidization. A "pulsed-bed" ALD reactor (Fig. 3b) has been proposed to resolve the dilemma.[18] When the precursor is introduced, the valve at the suction end is closed simultaneously, and the pressure difference between the two ends of the reactor generates a large pulse of gas flow, which blows up and agitates the powder bed. Compared to conventional fluidized bed reactors and processes, this reactor and process design may significantly reduce the consumption of precursors and carrier gas.

Rotary ALD reactors for fabricating large quantities of powder samples were also reported.[19] In a typical design (Fig. 4a), the powder was contained in a porous cylindrical stainless-steel drum inside a vacuum chamber, which was driven through a magnetically coupled rotating engine. The rotation speed was adjusted and a centrifugal acceleration less than 1 G was obtained, thereby the powder bed was agitated by continuous "avalanche". Compared with FBRs, in the rotary ALD reactor static reactant exposure and agitation of the powder bed are allowed simultaneously, the particle agitation provided by rotation improves contact between the particles and the reaction gases, and does not require continuous flow of gas for fluidization, therefore longer precursor residence time and better utilization of the precursors can be obtained.

A new reactor design named rotating fluidized bed, which combines the advantages of fluidized bed reactor and rotary reactor, has been proposed. Duan *et al.* demonstrated ALD of alumina on a silica powder using the rotating fluidized bed reactor (Fig. 4b).[20] The rotating fluidized bed reactor provides centrifugal force that assists fluidization of particles, and the gasless fluidization may solve the problem of low precursor utilization efficiency.

Recently, the concept of spatial ALD has also been introduced to fabricate powder materials. As a most special feature of spatial ALD, the two ALD half reactions are spatially separated from each other, so that no pumping or purging steps are required.[21,22] Van Ommen *et al.* proposed a novel spatial ALD reactor for catalyst preparation based on pneumatic transportation.[23] As shown in Fig. 4c, the spatial ALD reactor includes three parts: (i) the heating zone, (ii) the reaction zone for the first half reaction, and (iii) the reaction zone for the second half reaction. Different reactants were injected at the beginning of each reaction zone. With the N_2 flow, particles could be suspended and be transported from one reaction zone to the other. Using the spacial ALD reactor, platinum (Pt) nanoclusters with a diameter of about 1 nm were deposited on P25 titanium dioxide (TiO_2) nanoparticles.

Despite the limitations, a lot of lab-scale research on ALD powder fabrication is carried out with fixed bed ALD reactors, due to the fact that most commercially available ALD systems are only equipped with fixed bed reactors primarily designed for coating flat substrates. While for most fundamental research projects only a small amount of sample is needed, to develop practical applications of ALD for powder materials, research on ALD reactors capable of fabricating large quantities of powders and reducing the assumption of precursors is indispensable. To achieve these goals, innovations on reactor designs which can improve the gas–solid mass transfer, and the development of more efficient solid state precursor supply systems, are most important tasks.

3. Applications

3.1 Stabilization and passivation of particles

Owing to their excellent barrier properties, ALD films have been applied to flat substrates for the purpose of surface protection or stabilization. This advantage could also be applied to powder materials. The dense ALD film produced on the surface of particles

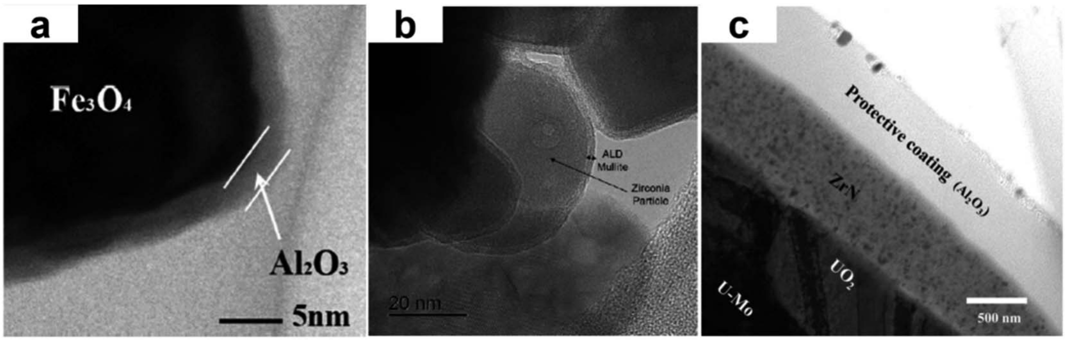

Fig. 5 (a) Bright-field TEM image of 50-cycle ALD Al_2O_3 coated Fe_3O_4 NPs; Reprinted with permission from ref. 24. Copyright (2016), American Vacuum Society. (b) HRTEM image of ALD mullite film on zirconia NPs; Reprinted with permission from ref. 26. Copyright (2018), John Wiley and Sons. (c) Bright-field TEM image of ALD ZrN film and U–Mo interface. Reprinted with permission from ref. 33. Copyright (2019), Elsevier.

could provide a unique surface sealing function, which would effectively isolate the underlying material from the environment and thus improve the stability of the particles. Al_2O_3 was the most widely used ALD coating material for surface passivation against oxidation, high temperature, moisture, corrosion and so on, due to its compactness and mature technology. In the past decade, more and more researchers have tried other oxide materials, such as TiO_2, ZrO_2, SiO_2, and nitride materials such as ZrN, as environmental barrier coatings (EBCs). The uniform surface coverage and precise thickness control of ALD could help minimize the content of surface modification material. This is essential for applications in which bulk properties of the original materials need to be maintained as much as possible.

Iron(II,III) oxide (Fe_3O_4) nanoparticles (NPs) are widely used in magnetism related fields, however, in atmospheric conditions Fe_3O_4 NPs tend to be spontaneously oxidized to Fe_2O_3 and lose their magnetization. Using a rotating fluidized bed ALD reactor, Duan *et al.* deposited uniform and pinhole-free Al_2O_3 films onto the Fe_3O_4 nanoparticles (Fig. 5a).[24] Thermogravimetric analysis showed that a 5 nm-thick ALD Al_2O_3 film effectively protected Fe_3O_4 nanoparticles from spontaneous oxidation, without losing the magnetic properties. Similarly, Cremers *et al.* applied ALD Al_2O_3 coatings on micron-scale Fe and Cu powders to improve their oxidation resistance.[25] For the Cu powder, an 8 nm ALD Al_2O_3 film can increase the oxidation temperature by 200 °C, while for the Fe powder, a 25 nm Al_2O_3 film is required to obtain a similar oxidation resistance effect.

Hoskins *et al.* reported the synthesis of mullite (Al_2O_3–SiO_2) films on zirconia and silicon carbide powders through ALD for the purpose of high temperature oxidation resistance (Fig. 5b).[26] Trimethyl aluminum (TMA), water, *tris*-dimethylaminosilane (TDMAS), and H_2O_2 were used as the reactants, and the films were annealed at 1500 °C for 5 hours to be converted to the mullite phase. Reduced oxidation of silicon carbide by up to 62% could be obtained with a 10 nm ALD alumina film. Compared with the ALD alumina film, 1.5 times thicker mullite film is needed to achieve a similar high temperature oxidation resistance effect.

Titanium dioxide (TiO_2) is an excellent white pigment. However, the high photocatalytic activity of TiO_2 under UV irradiation leads to inevitable degradation of surrounding materials, which seriously affects its application. In order to avoid the degradation caused by the photocatalytic activity of TiO_2, many efforts were made to passivate the TiO_2 particles through ALD. Alumina films were deposited on the TiO_2 nanoparticles by ALD in a fluidized bed reactor.[27] The coated TiO_2 particles showed reduced photo catalytic activity with the increasing film thickness. Liang *et al.* deposited aluminum alkoxide (alucone) films on TiO_2 particles using TMA and ethylene glycol as the precursors.[28] Methylene blue oxidation tests showed that the 20-cycle ALD alucone film could quench the photo catalytic activity of pigment-grade TiO_2 particles. With a fluidized bed ALD reactor, King *et al.* deposited 2 nm thick SiO_2 insulating films on TiO_2 particles using TDMAS and H_2O_2 as precursors at 500 °C.[29] H_2SO_4 digest experiment revealed that the ALD process enables high quality, fully dense SiO_2 film deposition on the substrates. The photocatalytic activity of pigment-grade anatase TiO_2 particles was reduced by 98% after the ALD surface passivation. A recent work by Guo *et al.* demonstrated that a 1 nm thick ALD Al_2O_3 layer could effectively inhibit the photo catalytic activity of rutile, anatase and P25 TiO_2 nanoparticles, without affecting the optical absorption.[30] Ceramic ALD coatings such as Al_2O_3 and SiO_2 can inhibit the photocatalytic activity by preventing the electrons and holes produced by ultraviolet absorption to migrate to the surface, and the large band gap of ceramic oxide materials ensures the optical transparency of the coating and thus retains the bright white color of TiO_2. Precise control on the thickness of the coatings allows TiO_2 particles to maintain the original gloss and brightness of the pigment while inhibiting the photocatalytic activity.

As a type of potential lighting material, fluoride phosphors have attractive optical properties. However, their sensitivity to moisture may lead to phosphor degradation, and the poor chemical stability limits their applications. ALD Al_2O_3 and TiO_2 layers were deposited onto fluoride phosphor particles to improve their chemical stability.[31] Both films could cover the surfaces of the fluoride phosphor particles. The ALD Al_2O_3 shells suffered from delamination and blistering after deposition, whereas ALD TiO_2 layers appeared conformal and uniform. With the ALD TiO_2 coating, the fluoride particles obtained enhanced adhesion with the hydrophobic shells and their chemical stability towards moisture was remarkably improved. In addition, for $SrAl_2O_4$-based long afterglow phosphor particles, the aqueous durability can be significantly improved by depositing nanoscale ALD Al_2O_3 or TiO_2 layers, as reported by Karacaoglu *et al.*[32]

In recent years powder ALD has shown potential in the field of nuclear energy. The precise processing ability and the relatively low deposition temperature are the key advantages of ALD for future applications in nuclear energy field. As an EBC material that could hinder the diffusion between U–Mo fuel and aluminum substrate, a ZrN layer is usually introduced on the surface of nuclear fuel particles by physical vapor deposition. However, due to the limitations of PVD methods, the binding between the ZrN film obtained by PVD and the substrate is relatively weak, and it is easy to delaminate under irradiation. ALD may provide a better solution than PVD. ALD zirconium nitride (ZrN) films were deposited onto natural uranium–molybdenum (U–Mo) based fuel particles (Fig. 5c) to form a diffusion barrier coating that could prevent the harmful interaction between the fuel and the aluminum matrix.[33] *In situ* heavy ion irradiation experiment showed that the ALD ZrN film significantly improved the irradiation stability of the fuel particles. During the extended storage process of spent nuclear fuel, helium gas accumulation from alpha decay could damage the structural integrity of the fuel. ALD Al_2O_3 layer could serve as a barrier for the retention of helium generated from fuel particles.[34] Surrogate micron-scale nickel particles were homogeneously coated with 3–20 nm thick Al_2O_3 films in a fluidized bed ALD reactor and were then loaded with helium at 800 °C in a tube furnace. Subsequent helium spectroscopy measurements showed that the ALD Al_2O_3 coating increased the helium storage capacity by up to two orders of magnitude compared to the uncoated nickel particles. Environmental barrier coatings that block hydrogen diffusion are necessary for preventing the embrittlement of uranium fuel substrate and avoiding corrosion. ALD tungsten nitride (WN) films were deposited on zirconia NPs and yttria stabilized zirconia micropowders.[35] Subsequent annealing was performed to produce a crystallized tungsten coating. Differential thermal analysis (DTA) test revealed that the reaction of hydrogen with the underlying material was delayed by the ALD film. To completely eliminate the reaction, thicker ALD film or more effective EBC should be selected.

Stabilization and passivation of particles is a universal requirement for a number of different areas. More examples on this topic will be further discussed in the sections of catalyst and energetic material.

3.2 Catalyst

ALD has been widely used in the field of catalysis. ALD enables precise fabrication of nano or sub-nano surface structures, which provides a powerful tool to synthesize model catalysts. For catalysis applications complete encapsulation of particles is usually not required. Clustered or island structures formed at the early stage of film nucleation are the most important reactive sites for catalytic reactions. In most cases only a few cycles of ALD are performed. On the other hand, supports for catalysts may have much more complicated structures as well as much larger surface areas than conventional solid particles. Consequently, in each ALD cycle a very long precursor exposure is usually needed to ensure saturated surface reaction. With the unique capability of ALD in atomic layer by layer fabrication of 3D structures, precisely controlled catalytic materials could be obtained, which are beneficial for establishing the correlation between structural and chemical properties, such as active components, particle size, surface chemical states, and exposed crystal facets and their catalytic performances. Many novel catalytic structures, such as core shell structures, partially embedded structures, single atom catalysts, bimetallic catalysts, ALD overcoatings, controlled micro environments, have been fabricated, for the purpose of improving the catalytic performances in terms of activity, selectivity, and stability.[36] In this section, examples will be categorized according to the type of substrate and the catalytic materials.

3.2.1 Metal ALD on oxide or carbon support. Supported noble metal catalysts are widely used in chemical and environmental industries. Since noble metals are very expensive, it is desirable to make the catalysts in a highly dispersed state to increase their efficiency. ALD is the perfect technology for this purpose. Noble metals are among the earliest discovered metal materials that can be synthesized by thermal ALD. Normally, the ALD film deposition processes of noble metals on metal oxide substrates follow the island growth mechanism.[37,38] That is, during the early stage of film growth, highly dispersed metal particles, rather than continuous metal films, are formed, which can be used as excellent active sites for catalytic reactions. In some cases, nucleation delay can be observed when a metal element is deposited on certain types of oxide supports. Nucleation delay refers to an incubation period at the early stage of an ALD process, during which the film growth rate is much lower than the normal deposition rate. The nucleation delay is related to many factors, such as surface chemical properties and reaction enthalpy changes. Sometimes, before depositing precious metal species, an ultra-thin oxide layer such as alumina or titanium dioxide is first deposited on the surface of the support to overcome the nucleation delay or to facilitate metal growth. Examples on oxide ALD on oxide supports will be illustrated in details in the next sub-section. Many efforts have been made to deposit NPs, clusters, or single atoms of Pd, Pt, and other metals on a variety of support materials. The synthesized catalytic materials can be used for traditional heterogeneous catalysis, photocatalysis, or electrocatalysis reactions.

Feng *et al.* studied the nucleation and growth of ALD Pd films on different oxide substrates using palladium hexafluoroacetylacetonate ($Pd(hfac)_2$) and formalin as precursors.[39] Pd nanoparticles were deposited on ZnO and Al_2O_3 coated mesoporous silica gel and their catalytic performances were evaluated in methanol decomposition. The ALD Pd/Al_2O_3 catalyst exhibited high activity, while the ALD Pd/ZnO catalyst deactivated rapidly. *In situ* extended X-ray absorption fine structure (EXAFS) measurements revealed that during methanol decomposition, the Pd species supported on ZnO could “dissolve” into the matrix, leading to gradually diminished activity. An overcoating layer of ALD Al_2O_3 could bind to Pd species and effectively prohibit the loss of activity. Based on a similar strategy, ultra small Pd particles were synthesized on alumina support by low temperature Pd(hfac)$_2$ exposure followed by depositing ALD Al_2O_3 protective coatings.[40] In the following high temperature reduction step, the size of the Pd particles could remain unchanged. Gong *et al.* studied the size distribution of Pd particles deposited on an activated carbon (AC) support by ALD.[41] The AC support was pre-treated by acid reflux and high temperature calcination to tailor the surface functional groups. The average size of Pd NPs supported on AC was determined by the number of ALD cycle as well as the type and concentration of functional groups on the support (Fig. 6). Pd NPs were also deposited on Fe_2O_3 modified AC to form a large surface area magnetic Pd/Fe_2O_3/AC catalyst.[42] The AC support was modified by Fe_2O_3 ALD followed by Pd ALD. In hydrodechlorination of 1,4-dichlorobenzene the Fe_2O_3 species in close contact with Pd effectively prevented the metal species from being poisoned by chloride ions and thus enhanced the catalytic performance. In another case, Gong *et al.* deposited TiO_2 coatings inside the mesopores of a silica molecular sieve MCM-41.[43] Then ALD of Pd was performed to produce a highly dispersed Pd/TiO_2/MCM-41 catalyst. In selective hydrogenation of acetylene, the ALD Pd/TiO_2/MCM-41 catalyst showed very good conversion and selectivity to ethylene. The spatial confinement effect from internal channels of the molecular sieve leads to a narrow size distribution of Pd nanoparticles and effectively prevents sintering of particles during the high temperature treatment. The small, uniform Pd nanoparticles densely distributed in the *meso*-pores of MCM-41 significantly enlarged the number of active sites and lowered the reaction temperature.

Platinum (Pt) is also widely used as an industrial catalyst in the areas of fuel cell, automotive and petroleum industries, despite its high price. Lashdaf *et al.* proposed for the first time that ALD could be used to deposit Pt on silica or alumina support to make a supported catalyst.[44] Goulas *et al.* reported the method to synthesize platinum nanoclusters on TiO_2 NPs with an atmospheric pressure fluidized bed ALD reactor using trimethyl methylcyclopentadienyl platinum ($MeCpPtMe_3$) and ozone as reactants.[45] Homogeneously distributed and highly dispersed Pt nanoclusters with a narrow size distribution were obtained. Using the same ALD reaction Pt NPs were also uniformly supported on carbon nanotubes (CNT).[46] The Pt/CNT catalyst showed excellent catalytic performance in the hydrolysis of ammonia borane. Covering the Pt/CNT with a porous ALD TiO_2 layer could further improve the durability of the catalyst. Dendooven *et al.* reported a strategy to achieve independent control over the Pt particle size and coverage by combining two distinct ALD processes of Pt.[47] The particle density was controlled by tuning the ALD cycle using $MeCpPtMe_3$ and oxygen as the precursors, while the particle size was controlled by subsequent growth using the same Pt precursor and nitrogen plasma. X-ray fluorescence (XRF) and grazing incidence small-angle X-ray scattering (GISAXS) measurements confirmed a good control of the loading, density, and average size of Pt particles. This method demonstrates the feasibility of independently controlling the size and coverage of metal particles by combining different ALD processes, which is usually difficult to achieve through a single ALD process. Leus *et al.* reported the synthesis of ALD Pt NPs confined in a metal organic framework (MOF) material.[48] ALD of Pt was conducted at 200 °C using $MeCpPtMe_3$ and O_3 as precursors. The utilization of O_3, which is a more powerful oxidizer than oxygen, makes it possible to remove the ligand at a lower temperature, which may help prevent coalescence of Pt particles. The structure of the metal organic skeleton was well maintained during the ALD process. By XRF and TEM analysis, it was confirmed that Pt NPs were highly dispersed in the MOF structure. The obtained catalyst exhibited excellent activity in hydrogenation of different linear and cyclic olefins.

High cost is the major drawback of noble metal catalysts. Since only the atoms exposed on the surface of catalyst particles can participate in the catalytic reaction, researchers have been trying to downsize catalyst particles to maximize the utilization of noble metal species. To this end, fabricating single atom noble metal catalyst would be an ideal solution. However, the synthesis and stabilization of single atom catalyst is a big

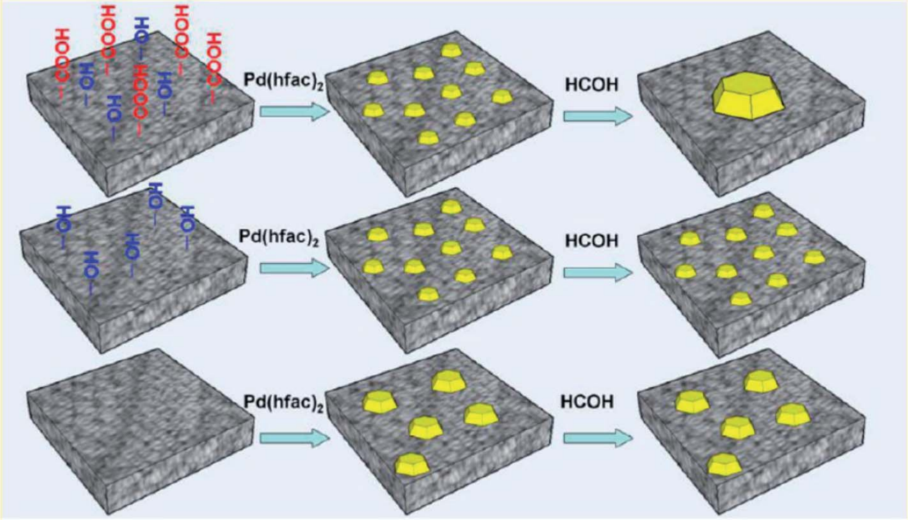

Fig. 6 Schematic representation on effects of surface functional groups on Pd particle size synthesized by ALD. Reprinted with permission from ref. 41. Copyright (2015), American Chemical Society.

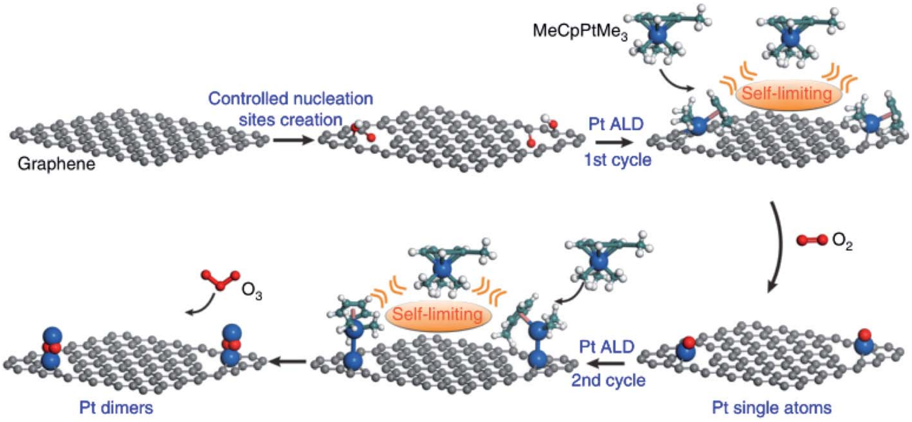

Fig. 7 Schematic illustration of the bottom-up synthesis of dimeric Pt_2/graphene catalysts. Creation of isolated anchoring sites on pristine graphene; followed by one cycle of Pt ALD at 250 °C for the formation of Pt single atoms; the second cycle of Pt ALD was performed at 150 °C to selectively deposit the secondary Pt atoms on the preliminary ones for the formation Pt_2 dimers. The balls in cyan, white, red, and blue represent carbon, hydrogen, oxygen, and platinum while the ball in gray represents carbon atoms in the graphene support. Reprinted with permission from ref. 54. Copyright (2017), Springer Nature.

challenge, because metal atoms are extremely mobile and are very easy to sinter under reaction conditions. One possible way is to anchor the single atoms into the surface defects of oxide supports. ALD has been proved to be an important method for the synthesizing and investigating of single atom catalyst.[49] Single-atoms and sub-nanometer clusters of Pt were supported on the surface of graphene nanosheets using ALD.[50] Very limited anchoring sites for Pt precursor were distributed on the inert surface of graphene, thus effectively prevented agglomeration of Pt atoms. Compared with traditional Pt/C catalysts, these catalysts showed higher activity and excellent CO tolerance in methanol oxidation reaction, which was attributed to low-coordinated and unsaturated 5d orbitals of the single Pt atoms. Using a similar strategy, Cheng *et al.* synthesized nitrogen-doped graphene nanosheets supported single platinum atoms and clusters for hydrogen evolution reaction (HER) through ALD.[51] Compared with commercial Pt/C catalysts, the catalytic activity was significantly improved by up to 37 times. Pt single atoms were also deposited on the MOF-derived N-doped carbon through ALD to produce single-atom catalysts. The catalyst showed 6.5 times higher activity in oxygen reduction reaction (ORR). The electronic structure of Pt single atoms can be tuned by the co-adsorption of hydroxyl and oxygen, which significantly reduces the free energy change of the rate-determining step and thus enhances the ORR activity.[52] From the above examples, it can be noticed that the selection of support materials with defect sites, such as nitrogen-doped graphene nanosheets and MOF-derived N-doped porous carbon, may be an effective way to synthesize and stabilize single atoms through strong metal support interaction.

To compare the effects of single atom and nanoparticle catalysts, Pt was loaded onto mesoporous zeolite HZSM-5 with different ratios of Pt single atoms to nanoparticles using ALD at high temperature or solution grafting at room temperature.[53] Catalytic performances in CO oxidation and low temperature water–gas shift (WGS) reactions were studied. IR spectroscopy characterization using CO as a probe molecule confirmed that the activity for CO oxidation and low temperature WGS reaction were only observed with Pt nanoparticles but not with Pt single atoms. This result demonstrates that the strategy of using single atoms to improve the catalytic efficiency may not work for all reactions. Yan *et al.* reported the method of synthesizing Pt_2 dimers on graphene using ALD.[54] A schematic illustration of the synthetic process is shown in Fig. 7. Pt single-atoms were deposited on the nucleation sites created before, then secondary Pt atoms were attached selectively to the Pt atoms previously deposited. In the reaction of ammonia borane hydrolysis, the Pt_2/graphene catalyst showed impressive activity, which was about 17 times higher than graphene supported Pt_1 single-atoms and 45 times higher than Pt NPs, respectively. The decreased adsorption energy of ammonia borane and H_2 molecules on Pt_2 dimers may be the main reason for the promoted activity.

Single atom Pd catalysts could also be fabricated by ALD. A method of synthesizing single atom Pd_1/graphene catalyst (Fig. 8) by performing one cycle of ALD Pd on high temperature annealed graphene was reported.[55] In selective hydrogenation of 1,3-butadiene, the Pd_1/graphene catalyst showed ~100% butene selectivity with 95% conversion under a mild reaction condition. The high selectivity may be attributed to the changed adsorption mode of 1,3-butadiene as well as the enhanced steric effect on Pd atoms. The same group also synthesized single atom Pd_1/C_3N_4 catalyst for acetylene hydrogenation reaction, and enhanced selectivity to ethylene and coking resistance were obtained.[56]

Besides noble metal catalysts, some other active transition metal elements, including Ni, Cu, Fe, and Co, can also be synthesized by ALD. Similar to ALD noble metal catalysts, highly dispersed transition metal NPs or clusters with precisely controlled structures could be generated on a variety of supports, and these highly dispersed metal species can effectively promote the efficiency of active materials. For example, a nickel (Ni) NP catalyst was prepared by performing ALD of Ni on a porous γ-Al_2O_3 powder using bi(cyclopentadienyl) nickel ($NiCp_2$) and hydrogen as precursors.[57] The γ-Al_2O_3 supported Ni NP catalyst exhibited both high activity and stability in high temperature dry reforming of methane (DRM). The improved

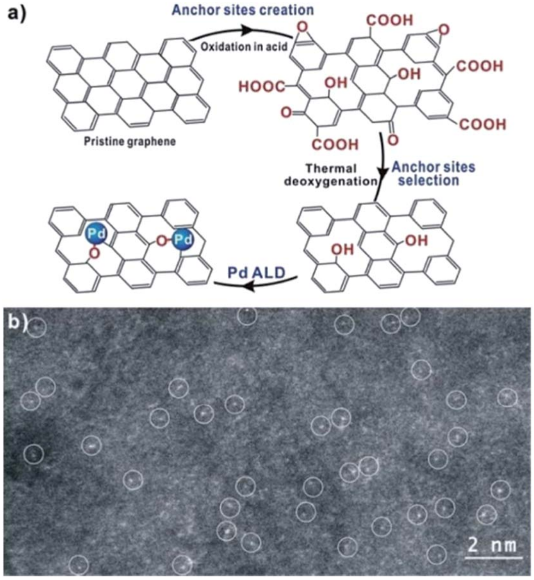

Fig. 8 (a) A schematic illustration of single-atom Pd_1 catalyst synthesized on high temperature treated graphene through anchoring site creation, selection, and Pd ALD. (b) Representative HAADF-STEM images of Pd_1/graphene (atomically dispersed Pd atoms are highlighted by white circles). Reprinted with permission from ref. 55. Copyright (2015), American Chemical Society.

performance was attributed to the formation of $NiAl_2O_4$ that could be reduced to highly dispersed metallic Ni during the DRM reaction. Through ALD of Cu on a mesoporous silica using $Cu(thd)_2$ (thd = 2,2,6,6-tetramethyl-3,5-heptanedionate) and ozone as precursors, a Cu/SiO_2 catalyst was prepared.[58] In low temperature WGS reaction, the ALD Cu/SiO_2 catalyst exhibited excellent activity, which was related to defect sites on small Cu particles or clusters that may induce strong interactions with the support.

3.2.2 Oxide and sulfide ALD on oxide, carbon, or polymer support. Metal oxide (MO) is another class of widely used heterogeneous catalyst. MO catalysts can not only be used for redox reactions, but can also be used for acid–base catalyzed reactions. Most MO materials can be synthesized by ALD. Usually no nucleation delay is observed when a MO is deposited on a MO substrate. By depositing one or several ALD cycles of MO on the surface of oxide, uniformly distributed and highly dispersed MO species can be obtained; upon increasing the ALD cycle number, the MO species will coalesce to form a continuous thin film, while the fundamental structure of the original support is maintained. The deposited MO species may directly be used as the active site or as a new substrate for introducing the desired active site-support interaction.

Porous alumina particles were synthesized by depositing thin films of Al_2O_3 on a highly porous poly styrene-divinylbenzene (PS-DVB) template *via* ALD, followed by high temperature calcination to remove the organic template.[59] The deposition was held at 33 °C with TMA and water as precursors in a fluidized bed reactor. The obtained porous Al_2O_3 particles had a surface area of 80–100 $m^2\ g^{-1}$ and could be used as a template or support material.

VO_x were deposited onto an alumina support by ALD, using vanadium oxytriisopropoxide (VOTP) and hydrogen peroxide (H_2O_2) as precursors.[60] A series of VO_x/Al_2O_3 catalysts with precisely controlled structures were synthesized by varying the number of VO_x ALD cycle. In the reaction net work of cyclohexane ODH, mono vanadate was found to favor the formation of olefin, while poly vanadates facilitated the direct conversion from cyclohexane to benzene.[61] Catalytic performances of the series of ALD VO_x/Al_2O_3 catalysts were also investigated in oxidative dehydrogenation of ethylbenzene with CO_2 (CO_2-ODEB). In this reaction, isolated VO_x monomer was discovered to be more active and stable than the polymeric VO_x and crystalline V_2O_5. V–O–Al bonds were considered as the major active sites for CO_2-ODEB.

NiO was deposited on mesoporous SiO_2 by means of ALD using $NiCp_2$ and H_2O as precursors.[62] The NiO NPs were uniformly distributed on the mesoporous SiO_2 support. The ALD NiO/SiO_2 catalyst was very effective for catalyzing toluene combustion reaction below 200 °C. The high activity was attributed to the large surface area of the mesoporous SiO_2 substrate, which could significantly increase the loading of highly dispersed catalytic species and accelerate the oxidation of toluene by enhancing the diffusion of adsorbed toluene from SiO_2 to NiO. Similarly, carbon nanotube (CNT) supported NiO NPs were prepared through ALD using $NiCp_2$ and O_3 as precursors.[63] Due to the lack of defect sites on CNT, it is difficult to directly grow oxides on the surface of CNT. In this study, O_3 played both the roles of the defect forming agent and the oxygen source. In the electro-oxidation of methanol, the ALD NiO/CNT catalyst showed significantly improved electrochemical catalytic activity and stability. The enhanced catalytic performance was resulted from the strong interaction between NiO and CNTs, which prevented NiO NPs from dissolution, Ostwald ripening, or aggregation during the reaction.

Singh *et al.* performed ALD of TiO_2 to fabricate the surface of a fibrous nano-silica (KCC) support using titanium tetraisopropoxide ($Ti(OiPr)_4$) and H_2O_2 as precursors to make an effective photocatalyst.[64] Conformal coatings of TiO_2 on KCC were obtained. After proper heat treatment uniformly dispersed ultra small TiO_2 NPs were formed. In photocatalytic degradation of organic pollutants, activity of the ALD TiO_2/KCC catalyst was much higher than many other reported catalysts. The superb catalytic performance was resulted from the combined effects of the unique mesoporous structure of KCC that facilitated diffusion of reactants and the size quantization effect of TiO_2 NPs. Chen *et al.* proposed a strategy to synthesis carbon supported nanoporous nitrogen-doped TiO_2 photocatalysts using an ABCB four-step ALD reaction sequence in which titanium tetrachloride ($TiCl_4$, precursor A), ethanolamine (precursor B), and malonyl chloride (precursor C) were used as the precursors.[65] After 200 cycles of deposition, the obtained film was annealed at 350 °C and the nanoporous structure was formed. The nanoporous catalyst exhibited excellent photocatalytic activity in the degradation of methylene blue even with visible light radiation. The photocatalytic activity of SnO_2 NPs can be enhanced by forming core–shell NPs through ALD, as reported by Podurets *et al.*[66] Ultra thin (<10 nm) ZnO and TiO_2

films were deposited onto SnO_2 NPs. In photocatalytic degradation of methylene blue under UV-Vis irradiation, full degradation was achieved within 10 min using the core–shell catalysts. The promoted photocatalytic activity was attributed to the core–shell structure which adjusted the band gap value.

Highly dispersed ZnO species were deposited onto ZSM-5 and Y zeolites by ALD using diethyl zinc (DEZ) and H_2O as precursors.[67] With the incorporation of ZnO, Brønsted acid sites on Y zeolite were completely removed, while those on ZSM-5 were only partially removed. Activities of both types of zeolites were significantly enhanced in the reaction of propane dehydrogenation and aromatization. ZnO species (Lewis acid sites) promoted the dehydrogenation reaction, while subsequent oligomerization and cyclization reactions required participation of Brønsted acid sites.

Iron oxide NP catalyst supported on reduced graphene oxide (rGO) was prepared by ALD using bi(cyclopentadienyl) iron ($FeCp_2$) and oxygen as precursors.[68] Fe_2O_3 NPs with a narrow size distribution were homogenously dispersed on the rGO nanosheets. The ALD Fe_2O_3/rGO catalyst exhibited high catalytic activity for thermal decomposition of ammonium perchlorate (AP). The enhanced catalytic performance was attributed to the optimized spatial distribution of Fe_2O_3 NPs supported on the rGO nanosheets and the synergistic effect between them. Porous Fe_2O_3 nanotubes were prepared by ALD using different kinds of iron containing metal–organic compounds and organic constituents as precursors on a carbon fiber support.[69] After proper high temperature annealing porous nanotubes with tunable pore size and α–γ phase junctions were obtained. The porous Fe_2O_3 nanotubes exhibited superior activity for photo-Fenton reaction. The porous nanotubes produced using iron *tert*-butoxide (ITBT) and ethylene glycol (EG) as precursors showed the highest photo catalytic activity.

In addition to metal oxides, sulfide materials grown by ALD have aroused attention in the field of catalysis. The ALD processes of metal sulfide materials usually use metal organic compounds and hydrogen sulfide (H_2S) as precursors.[70] The procedures of metal sulfide ALD are very similar to those of metal oxide ALD. Cobalt sulfide was deposited onto a MOF material named NU-1000 using bis(*N*,*N*′-di-*i*-propylacetamidinato) cobalt(II) ($Co(amd)_2$) and H_2S as precursors.[71] Cobalt sulfide was uniformly deposited throughout the MOF structure without destroying the crystallinity and porosity of the support. The resulting ALD in MOF (AIM) material exhibited higher catalytic efficiency than cobalt oxide and CoS_x reference materials in selective hydrogenation of *m*-nitrophenol to *m*-aminophenol, as a result of the high dispersity of CoS_x sites. The same group also reported the synthesis of NiS-AIM catalysts.[72] Few-atom clusters of nickel sulfide was synthesized on the NU-1000 MOF support by ALD using bis(*N*,*N*-di-*tert*-butylacetamidinato) nickel(II) and H_2S as precursors. The NiS-AIM catalyst exhibited excellent activity in a photocatalytic hydrogen evolution reaction (HER). The rate of H_2 production reached 4.8 mmol g^{-1} h^{-1}. A NU-1000 MOF supported iron-thiolate photocatalyst was also synthesized through an MLD process, using iron amidinate coordination complex and 1-dodecanethiol as precursors.[73] When exposed to light, the MOF supported iron-thiolate catalyst can convert nitrate into ammonium ions. These results indicate that depositing catalytic components on the active nodes of chemically stable MOF materials using ALD or MLD is a very promising method of synthesizing MOF supported catalysts.

Molybdenum disulfide (MoS_2) has been considered an ideal material to replace noble metals as a high-performance electrocatalyst in HER, due to its low cost and high activity. NiS_x@MoS_2 heterostructure electrocatalysts with controllable interface properties were synthesized by depositing NiS_x on MoS_2 nanosheets using ALD.[74] Compared with single-phase MoS_2 and NiS_x, NiS_x@MoS_2 heterojunctions have lower over potential and faster reaction kinetics, which greatly enhanced the HER activity. The improved catalytic performance is attributed to the optimized adsorption of reaction intermediates and the promoted charge transfer near the MoS_2/NiS_x interface. In addition to the high activity, NiS_x@MoS_2 heterojunctions also showed high stability in the alkaline medium.

Metal sulfides synthesized by ALD are very promising catalytic materials. However, in most ALD processes of metal sulfides, highly toxic, explosive, and corrosive H_2S is used as the sulfur precursor, which seriously limits the large-scale application. In order to solve this problem, an organic sulfur precursor, di-*tert*-butyl disulfide (TBDS) was developed to replace H_2S for metal sulfide ALD.[75] It has been proved that the new ALD process using aminated nickel and TBDS precursors has ideal ALD growth behaviors, and high quality NiS_x films can be prepared. The new ALD process of metal sulfide that avoids the use of H_2S will greatly favor the applications of ALD metal sulfides in catalysis and nanoscience.

3.2.3 Metal ALD on metal. Bimetallic catalysts can exhibit better catalytic performances than their parent monometallic counterparts, on account of the synergistic effect of the two components.[76] Bimetallic catalysts can be conveniently synthesized *via* ALD by sequentially depositing two different metallic materials under controlled conditions. By varying the cycle number of different ALD processes, bimetallic catalysts with different composition and structure can be precisely produced. However, the synthesis of bimetallic catalysts through ALD might be challenging when the two metals do not share a common ALD temperature window or the surface chemical reactions are incompatible. It is also difficult to ensure that the second metal species grow only on the surface of the first metal particles and not on the support.[76] In the following section different strategies to selectively deposit the second metal on the primarily metal particles to form bimetallic catalysts will be introduced.

In the work of Christensen *et al.*, a method of synthesizing Pt–Ru NPs by sequential ALD of Pt and Ru on an Al_2O_3 powder was demonstrated.[77] The composition of the NPs could be controlled by varying the ratio of Pt to Ru ALD cycles, while the particle size could be controlled by the total number of ALD cycles. These bimetallic catalysts exhibited improved activity for methanol decomposition compared to a mixture of supported Pt and Ru NPs.

Atomic scale controllable synthesis of Pd/Pt and Pt/Pd core–shell NPs *via* area-selective ALD was reported.[78] The method involves pre-treating the substrate using self-assembled monolayers (SAMs) of octadecyl trichlorosilane (ODTS). The

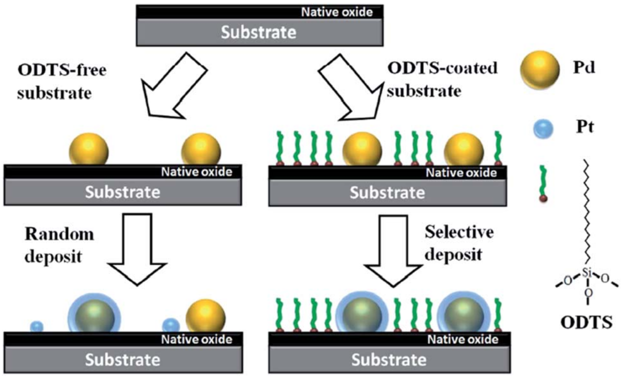

Fig. 9 Schematic illustration for fabricating core–shell NPs through area-selective ALD on ODTS modified substrate. Reprinted with permission from ref. 78. Copyright (2015), Springer Nature.

formation time of the SAM was controlled to obtain pinholes, in which hydroxyl (–OH) groups were exposed as the intended nucleation sites for metal species. Since the surface ODTS SAMs can effectively prevent the generation of new nucleation sites, the second metal was selectively deposited on the previous nucleation sites to form the Pd/Pt and Pt/Pd NPs with uniform core–shell structures and a narrow size distribution (Fig. 9). The SAMs-assisted area selective ALD is a typical strategy to achieve selective ALD growth. This method can be easily applied to synthesize other core–shell structured NPs with different components, which provides a convenient and flexible way of manufacturing novel nano structures.

In an ALD process nucleation of metal on the surface of different supports is dependent on reaction conditions such as atmosphere and temperature. Lu *et al.* reported low temperature selective ALD to synthesis supported bimetallic NPs.[79] With careful selection of the co-reactants and deposition temperature, the secondary metal would prefer to grow on the surface of primary metal NPs, rather than on the oxide support (Fig. 10).

ALD can also be combined with other techniques to synthesize supported bimetallic catalysts. In the report of Wang *et al.*, an Au/SiO_2 catalyst was first synthesized using a deposition–precipitation method, then Pd was selectively deposited only on the surface of Au NPs by choosing a proper deposition condition.[80] Thus Pd@Au core–shell bimetallic NPs were formed on the silica support. Atomic level precise adjustment of the Pd shell thickness could be achieved by changing the Pd ALD cycle. In solventless oxidation of benzyl alcohol, the best catalytic performance was obtained with a Pd shell thickness of 0.6–0.8 nm due to the optimum synergistic effect between the two metals.

3.2.4 Oxide ALD on metal catalyst. Stability is an important specification for evaluating the performance of a catalyst. For many catalytic systems coking, leaching, and sintering of the active sites are the major causes for catalyst deactivation. By applying ALD coatings on the surfaces of metal catalysts, oxide or nitride layers can grow on specific sites of the particle surface, which will act as protective layers to prevent the catalyst particles from coking, leaching, or sintering. Many materials, such as Al_2O_3, TiO_2, MnO_x, ZrO_2, and so on, have been used as ALD overcoatings to improve the stability of the catalysts in many catalytic reactions. By optimizing the composition and

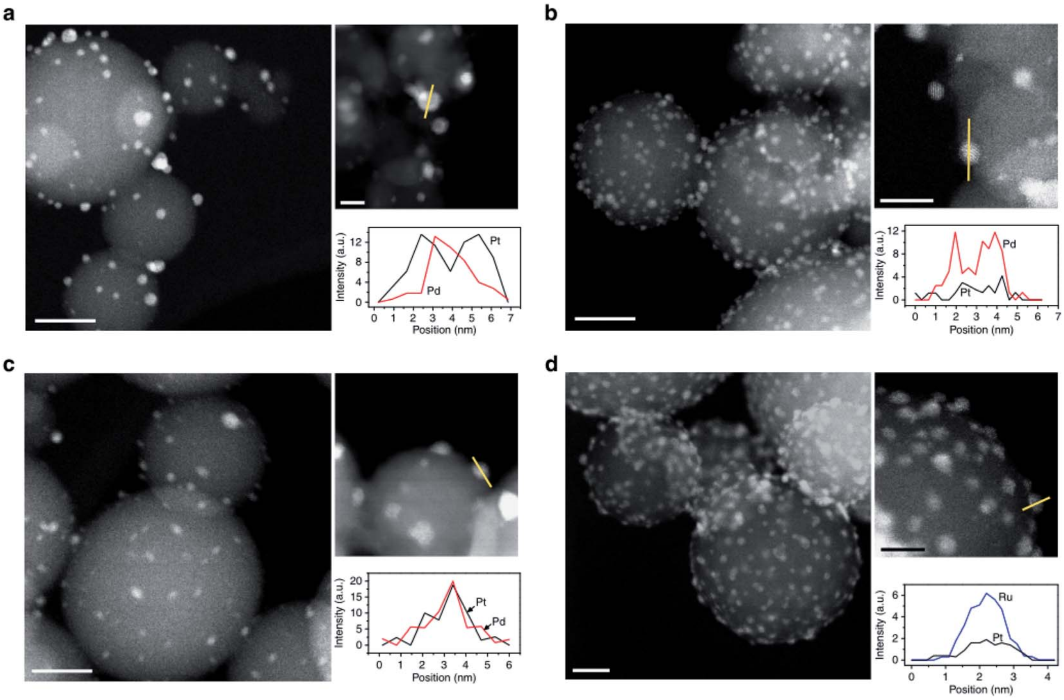

Fig. 10 Structures of ALD bimetallic NPs. Aberration-corrected HAADF-STEM images and corresponding EDS line profiles of (a), 5 Pd-core 15 Pt-shell; (b), 12 Pt-core 20 Pd-rich-shell; (c), 12 Pt 10 Pd alloy; and (d), 1 Pt-core 35 Ru-rich-shell bimetallic NPs on spherical alumina support. Reprinted with permission from ref. 79. Copyright (2014), Springer Nature.

structure of the overcoating layer, significantly enhanced stability of the catalyst can be achieved without affecting the activity.

Featuring the most typical ALD reaction, Al_2O_3 is the first reported ALD overcoating material. For example, supported palladium NPs were coated by 45 ALD cycles of Al_2O_3 at 200 °C using TMA and water as precursors.[81] The catalysts were tested in ODH of ethane to ethylene. After reaction at 675 °C for 28 hours, no visible change in the morphology of the catalyst was observed. Thermogravimetric analysis confirmed that coke formation was effectively inhibited. In another report, an effective approach to stabilize Pd/SiO_2 catalysts with porous ALD Al_2O_3 overcoating was demonstrated. Octahedra Pd NPs were supported on SiO_2 nanospheres, and then 40 cycles of Al_2O_3 ALD were performed to coat the Pd/SiO_2 catalyst.[82] Thermal treatment introduced pores to the Al_2O_3 overcoating and the embedded Pd particles were partially exposed. The ALD Al_2O_3 overcoated Pd/SiO_2 catalyst can efficiently catalyze methane combustion between 200 and 850 °C without significant deactivation. Applications of ALD Al_2O_3 overcoated Pd catalysts were also reported in many others catalytic reactions including methanol decomposition,[83] hydrogenation of furfural,[84] and hydrogenation of 1,3-butadiene.[85]

ALD coatings of MnO_x were also used to decorate Pd catalysts. Al_2O_3 supported Pd NP catalysts were prepared by wet impregnation, then ALD of manganese oxide was performed using tris(2,2,6,6-tetramethyl-3,5-heptanedionato)manganese(III) and ozone as precursors.[86] The ALD MnO_x coatings selectively passivated Pd (111) facets, and thus prevented decarbonylation of benzaldehyde and inhibited the formation of toluene byproduct, besides a high yield of benzaldehyde was obtained.

ALD Al_2O_3 coating was deposited on supported Pt NPs as the stabilizing layer against particle coarsening. *In situ* synchrotron grazing incidence small angle X-ray scattering measurements revealed that the ALD Al_2O_3 stabilizing layer successfully prevented Pt particle from coarsening during thermal annealing and improved the Pt surface accessibility.[87] A selective ALD method was developed to modify Pt NPs with nickel oxide (NiO_x) overcoating to improve the catalytic performance.[88] NiO_x can be selectively deposited on the low coordination sites of the Pt NPs during the initial growth period. Fourier transform infrared (FTIR) characterization and density functional theory (DFT) simulations proved that the source of selectivity is the intrinsic binding energy discrepancy of the nickel precursor on the platinum site. The ALD $NiO_x/Pt/Al_2O_3$ catalyst exhibited enhanced catalytic activity for CO oxidation, which could be attributed to the formation of a highly reactive metal oxide interface. Moreover, the sintering resistance ability of the overcoated catalyst was also significantly improved.

It is generally accepted that the catalytic activity of supported gold catalysts is largely dependent on the size of Au NPs, but the cause of this particle size effect is unclear. Yao *et al.* applied ultra thin TiO_2 overcoats of different thicknesses onto Au/TiO_2 catalysts with different Au particle size.[89] Combining the results of high-resolution TEM and XPS characterization and CO oxidation reaction, they proved that CO adsorption at the low coordination Au site is not the rate-determining step. Furthermore, the particle size effect in CO oxidation actually reflects the effects of perimeter of Au particles at the Au–TiO_2 interface. This example demonstrates that, with the help of highly controllable ALD method, many predetermined catalytic structures can be precisely synthesized, which are extremely useful for revealing the mechanism of catalytic reactions.

ALD overcoating can also be applied to non-noble metal catalytic systems. O'Neill *et al.* reported that copper catalysts can be stabilized by ALD Al_2O_3 overcoats.[90] In liquid-phase hydrogenation of furfural to furfuryl alcohol, the ALD Al_2O_3 overcoat decreased catalyst deactivation by preventing sintering and leaching of the metal catalyst (Fig. 11a). ALD Al_2O_3 and TiO_2 overcoats were also used to enhance the stability of a Cu based catalyst in furfural hydrogenation, and the effects of different types of overcoats were compared.[91] *In situ* TPR/TPO measurements revealed that TiO_2 had less modification effect on Cu than Al_2O_3. In the furfural hydrogenation reaction, the catalyst overcoated by ALD TiO_2 exhibited enhanced stability with unaffected activity.[92] After calcination at 500 °C, the interaction between the TiO_2 overcoat and the underlying catalyst was strong enough to inhibit the migration and steric hindrance of chromite, but it was much weaker than that between the Al_2O_3 overcoat and copper chromite, which could reduce the catalytic activity.

Protective ALD TiO_2 overcoats were applied to cobalt particles supported on TiO_2 (Fig. 11b and c).[93] For catalysts with ALD TiO_2 overcoats, high catalytic activity was maintained during aqueous-phase hydrogenation (APH) reactions. In contrast, the activity of the uncoated cobalt catalysts dropped quickly due to leaching of the active phase. The ALD TiO_2 overcoat stabilized cobalt catalysts were proved to be effective for APH of a series of

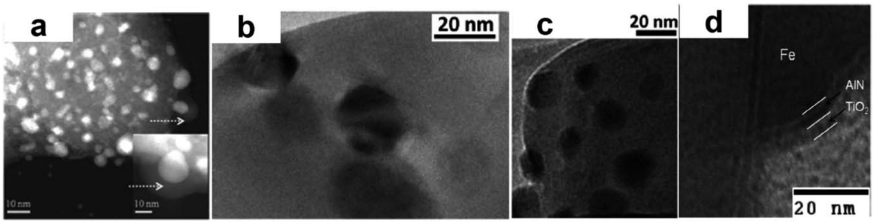

Fig. 11 TEM images of (a), AlN and TiO_2 bilayer film coated particles, dashed arrows point to the ALD overcoat; Reprinted with permission from ref. 90. Copyright (2013), John Wiley and Sons. (b) The $TiO_2/Co/TiO_2$ catalyst calcined at 873 K; (c), the used $TiO_2/Co/TiO_2$ catalyst. Reprinted with permission from ref. 93. Copyright (2014), Royal Society of Chemistry. (d) STEM image of TiO_2/AlN/Fe NPs. Reprinted with permission from ref. 94. Copyright (2010), American Chemical Society.

reactants including xylose, furfuryl alcohol, and furfural, in which the uncoated Co catalysts suffered from severe deactivation.

Iron-based magnetic photo-active NPs were modified by ALD of TiO_2 and aluminum nitride (AlN).[94] The iron NPs were produced by thermal decomposition of iron oxalate, and then TiO_2 films were deposited on the iron NPs in a fluidized bed ALD reactor at 100 °C using $TiCl_4$ and H_2O_2 as precursors. To prevent oxidation of iron particles, 100 cycles of AlN was performed at 250 °C with TMA and ammonia (NH_3) as precursors before the TiO_2 deposition (Fig. 11d). The AlN overcoat successfully inhibited iron oxidation while the magnetic moment was not affected. The ALD TiO_2 film provided photo catalytic activity for the magnetic NPs, as demonstrated by successful decomposition of a methylene blue (MB) solution under ultraviolet irradiation.

3.3 Energetic material

Energetic materials can store a large amount of chemical energy which can be quickly released upon thermal, mechanical, or electrical actuation. They have found extensive applications in explosives, propellants, and other energy related fields.[95] Thermal energy released from exothermic reactions of metal powder fuels has also been widely used. For example, thermite reaction, which is based on the solid state redox reaction between the metal fuel and the oxidizer, can release twice the amount of heat compared to conventional monomolecular energetic materials.[96] With the help of ALD, researches have been working on synthesizing new types of nanothermite materials and exploring proper surface modifications of metal fuels to improve their safety, stability, and energy release performances.

In general, the diffusion path between oxidant and fuel plays a decisive role in the rate and power of the thermite reaction. In order to obtain faster energy release and higher energy efficiency, oxidants and fuels should be mixed uniformly and the sizes of oxidant/fuel particles should be reduced to nano scale to shorten the diffusion path. Traditional methods of preparing energetic composites, such as sol–gel method, self assembly, and arrested reactive milling, fail to achieve accurate control of the composite structure or uniform mixing of the oxidant and the fuel. Core–shell structured nanothermite materials synthesized by ALD enable uniform combination as well as close contact of the oxidant and the fuel on nanometer scale. Ferguson *et al.* attempted to deposit oxidizer films on Al NPs to make nanothermites for the first time.[97] SnO_2 films were deposited on Al NPs using $SnCl_4$ and H_2O_2 as precursors in a fluidized bed ALD reactor. However, insufficient reactant exposure and unsaturated surface reaction led to a fuel/oxidizer ratio largely deviated from the stoichiometry of the thermite reaction. Nevertheless, SnO_2 coated Al NPs reacted much more quickly and violently than the uncoated Al particles. This work was complemented by Qin *et al.* in 2013.[98] By carefully adjusting the ALD pulse sequence of $SnCl_4$ and H_2O_2, perfect encapsulation of Al NPs by SnO_2 layers was achieved and Al@SnO_2 core–shell structured nanothermite material was synthesized (Fig. 12a and b). Laser ignition test showed that the resultant nanothermite reacted several times faster than the mechanical mixture of nanopowders. Similarly, Fe_2O_3 was also deposited onto the surface of Al NPs to produce Al@Fe_2O_3 core–shell structured nanothermite.[99] Compared with mechanically mixed Al–Fe_2O_3 nanopowders, the Al@Fe_2O_3 nanothermite had a lower ignition temperature, a larger energy release, and much faster reaction rate. The improved energy performance was attributed to the intimate contact and the uniform distribution of reactants on nanometer scale, which effectively reduced the average mass diffusion distance between the oxidizer and the metal fuel. Yan *et al.* reported the synthesis of a rGO/Al@Fe_2O_3 energetic composite by ALD.[100] Al NPs were first anchored on reduced graphene oxide (rGO) nanosheets, then Fe_2O_3 films were deposited onto the rGO/Al substrate by ALD, producing the rGO/Al@Fe_2O_3 energetic composite. The rGO/Al@Fe_2O_3 composite containing 4.8 wt% of rGO showed a 50% increase of the energy release compared to the Al@Fe_2O_3 nanothermite. The further improved energy performance was attributed to the dispersion of Al NPs on the surface of rGO nanosheets, which successfully prevent the agglomeration of Al particles during ALD of Fe_2O_3.

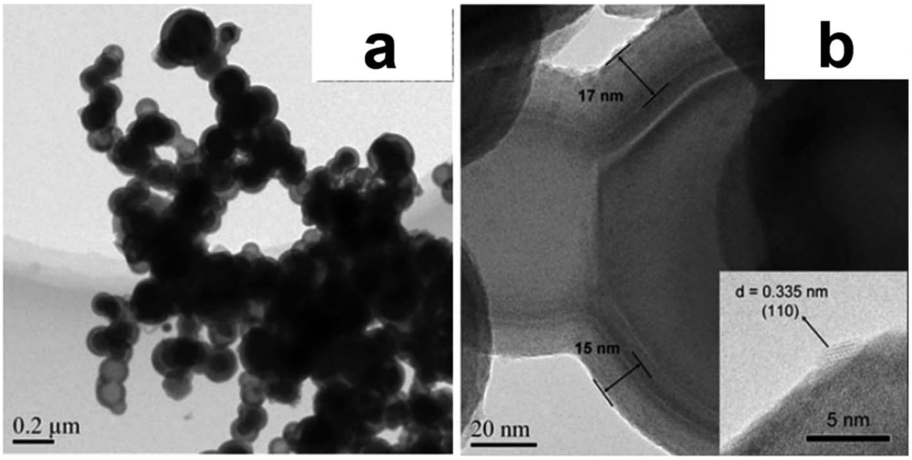

Fig. 12 SEM (a) and TEM (b) images of 225-cycle ALD SnO_2 coated Al nanopowder. Reprinted with permission from ref. 98, Copyright (2013), Springer Nature.

Surface passivation is important for energetic materials sensitive to air and water. Spontaneous combustion of energetic materials during storage, transportation, or handling are serious safety problems limiting the applications of novel energetic materials. Besides, composition change caused by oxidation or disintegration will reduce the energy density and change the energy release pattern. Consequently, sometimes it is necessary to carry out surface modification of high energy density materials to improve their safety and stability without deteriorating the energy performance. Aluminum hydride (AlH_3) is a very promising high energy material. However, its high reactivity with H_2O may lead to hydrogen release under ambient conditions. Chen *et al.* produced conformal passivation layers on α-AlH_3 particles by depositing Al_2O_3 films *via* ALD.[101] In hydrothermal aging tests, the passivated AlH_3 powder showed significantly improved stability with the presence of H_2O vapor. At elevated temperatures the dehydrogenation rate of the passivated AlH_3 is not much affected, indicating that ALD is a viable technique to stabilize AlH_3 without affecting its energy release capability.

Al powder is the most widely used metal fuel in many energetic systems, and the stability of Al particles is mainly due to the native oxide (Al_2O_3) layer. However, under certain conditions the surface native oxide layer is not able to stabilize Al particles. Al NPs were passivated using an ultrathin zirconia (ZrO_2) coating by ALD.[102] The hydrophobic ALD ZrO_2 passivation film successfully prevented the reaction between Al NPs and hot water at 80 °C (Fig. 13). The improved barrier property of ALD Al_2O_3/ZrO_2 laminated film might be a consequence of the $ZrAl_xO_y$ phase formation at the interface of Al_2O_3 and ZrO_2.

Zr powder is type of metal fuel featuring high volumetric energy density. However, safety issues such as uncontrolled oxidation and ultra-high electrostatic discharge (ESD) ignition sensitivity restrict the its applications. Qin *et al.*[103] applied molecular layer deposition (MLD) of polyimide to encapsulate Zr particles, and the following high temperature annealing converted the polymer films to carbon films. The polymer and carbon coatings greatly reduced the ESD sensitivity of the Zr powder without affecting the energy release. ALD Al_2O_3 coatings were also deposited on Zr particles. The ALD Al_2O_3 coating could form a dense gas diffusion barrier, which effectively suppressed oxidation of the Zr powder up to about 700 °C.[104] The ignition delay of the Zr powder was extended and the ESD ignition sensitivity was reduced.

So far, reports on surface modification of energetic materials using ALD are only about enhancing their stability and safety. In fact, the energy release processes of energetic materials are also closely related to surface physical and chemical properties, and ALD is an effective approach to regulate these properties. Therefore, ALD may also provide an important tool to control the energy release processes of various energetic materials by precise modifications on surface composition and structure.

3.4 Electrode material

Lithium-ion batteries (LIB) and capacitors (LIC) are among the most popular energy storage devices for applications in portable electronics and electrical vehicles. However, problems such as high cost, volume change during charging, degradation of electrodes, and safety concerns are limiting the applications of

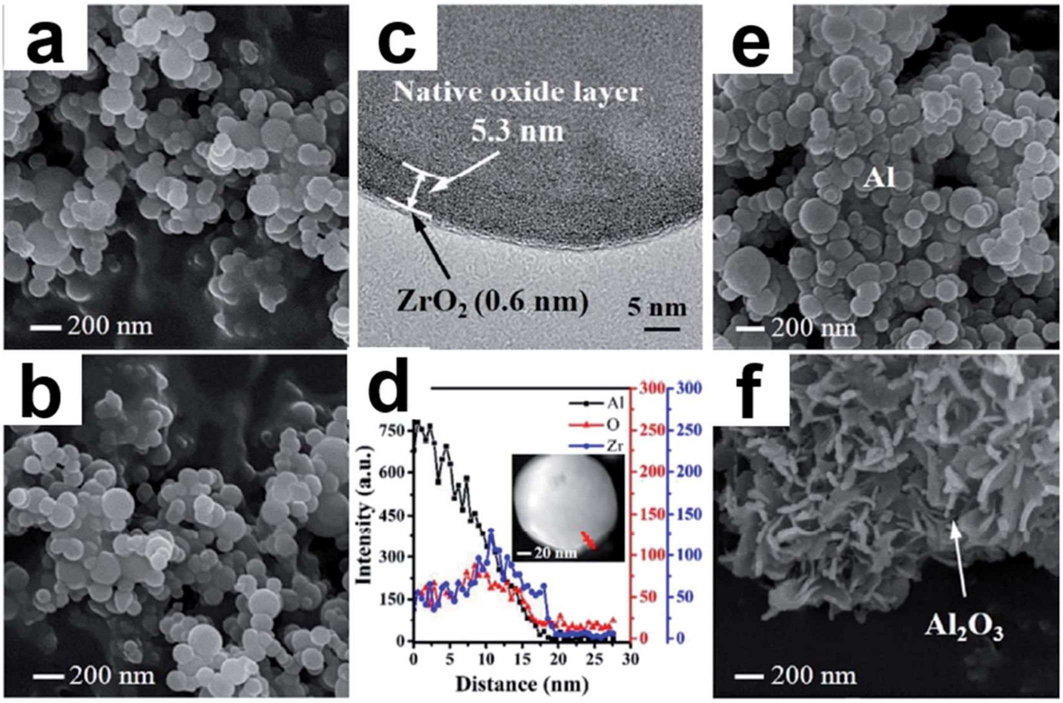

Fig. 13 SEM images of $Al@Al_2O_3@ZrO_2$-8 before (a) and after (b) stability test at 80 °C; TEM image (c) and element line scanning (d) of $Al@Al_2O_3@ZrO_2$-8 after stability test; SEM images of $Al@Al_2O_3@Al_2O_3$-50 before (e) and after (f) stability test at 60 °C. Reprinted with permission from ref. 102. Copyright (2018), American Chemical Society.

LIB and LIC.[105–107] Composition and structure of the electrode material, especially the surface chemistry between the electrode and the electrolyte greatly influences the electrochemical properties of batteries and capacitors.[108] By applying ultrathin ALD coatings of merely several nanometers, performances of the electrochemical materials can be remarkably improved. Many factors, such as reduced side reactions, promoted ion diffusion, and suppressed volume changes, may be responsible for the improved performances, however the exact mechanism still needs further investigation. In this section some typical applications of ALD for the fabrication of electrode materials used in LIB and LIC are introduced. Several examples of other energy devices, such as sodium ion batteries (SIB), solid oxide fuel cells (SOFC) and solar cells are also included. More detailed studies focusing on applications of ALD in the battery field can be found elsewhere.[106,107,109–111]

3.4.1 Surface modification of cathode material. For the cathode of LIB, side reactions occur when the cathode and the electrolyte directly contact, which may cause electrode degradation. Protection of the cathode material is a necessity. Metal oxides such as ZnO, Al_2O_3, ZrO_2, TiO_2, Fe_2O_3, and other materials including AlF_3, $FePO_4$, and $AlPO_4$ have been deposited by ALD on the cathode material as surface modification layers.

Previous studies have shown that the LIB performance can be improved if $LiCoO_2$ cathode material is coated with metal oxides using wet chemical techniques. In the research of Jung *et al.*, the $LiCoO_2$ powder was coated with an ultrathin Al_2O_3 film by performing only two cycles of ALD.[112] The ALD Al_2O_3 coated $LiCoO_2$ powder exhibited 89% capacity retention after 120 charge–discharge cycles, which is 100% higher than that of the bare $LiCoO_2$ powder. The underlying mechanism may be attributed to the barrier property of ALD Al_2O_3 film that can minimize Co dissolution or reduce surface electrolyte reactions. Li and co-workers studied the effects of ALD TiO_2, ZrO_2 and Al_2O_3 coatings on the electrochemical performance of $LiCoO_2$ electrode.[113] It was found that the improvement of battery performance is closely related to the type of coating material and that a dense coating on the $LiCoO_2$ powder may affect the diffusion of Li^+ ions and lower the battery performance.

A LIB cathode material $Li_{1.2}Ni_{0.13}Mn_{0.54}Co_{0.13}O_2$ was coated by nanolayers of Al_2O_3 and TiO_2 through ALD.[114] The ALD Al_2O_3 film was smooth and conformal, while the TiO_2 layer appeared to be composed of tiny particles. During repeated charging and discharging cycles, the ALD Al_2O_3 film improved the stability of the cell. The TiO_2 layer was more reactive with lithium and a Li_xTiO_2 interface was formed, which slightly increased the cell capacity but the repeated insertion/extraction processes of Li^+ ions caused erosion of the surface TiO_2 layer and resulted in decreased cell performance.

Lithium-rich layered materials are among the most competitive cathode materials for next-generation electric vehicles. However, a major problem of these materials is the oxygen release during initial charging, which may result in lower initial coulombic efficiency (CE), strong electrolyte oxidation, and thermal instability. According to the report of Xiao *et al.*,[115] the surface of a Li_2MnO_3 cathode material was protected by an aluminum phosphate ($AlPO_4$) coating synthesized by ALD using TMA, trimethylphosphate ($(CH_3)_3PO_4$, TMPO), and water as precursors. During the ALD process, part of the $C2/m$ Li_2MnO_3 phase transformed into a spinel phase which effectively suppressed the release of oxygen, and the initial CE could be significantly enhanced. Compared to the unprotected cathode material, ALD $AlPO_4$ coated cathode material was more stable at high temperatures.

Ultrathin cerium dioxide (CeO_2) films were coated on the surface of $LiMn_2O_4$ powder by ALD, using tris(i-propylcyclopentadienyl)cerium ($Ce(iPrCp)_3$) and deionized water as precursors.[116] The as-prepared cells performed high stability and high initial capacity retention after 1000 charge–discharge cycles. The improved cell performance was explained by suppression of the impedance rise and facile transport of the species.[117] ALD of CeO_2 was also applied to modify the surface of a Li-rich layered material made from $Li_{1.2}Mn_{0.54}Ni_{0.13}Co_{0.13}O_2$ (LRNMC) particles.[118] Compared with the uncoated LRNMC particles, the surface modified samples showed 8% higher capacity and significantly improved capacity retention after 400 charge–discharge cycles. The efficacy of the CeO_2 film was interpreted as increasing the substrate conductivity and blocking the dissolution of metal irons.

The most commonly used electrolyte material, lithium hexafluorophosphate ($LiPF_6$), may generate hydrofluoric acid (HF) when it encounters water. Therefore $LiPF_6$ may inevitably contain HF, which might etch metal oxide coatings. Metal fluorides could be more stable against HF corrosion than metal oxides. Jackson *et al.* developed the ALD process of AlF_3 in which TMA and TaF_5 were used as precursors.[119] Conformal AlF_3 films were deposited onto a $LiNi_{0.5}Mn_{0.3}Co_{0.2}O_2$ (NMC) Li-ion battery cathode material. The coin cell with coated cathode particles exhibited significantly improved charge capacity at high discharge rates.

Besides LIBs, cathode materials of other batteries or capacitors were also modified with ALD protective layers. For example, ALD Al_2O_3 layers were reported to be effective for enhancing the cyclic stability of a $Na_{2/3}(Mn_{0.54}Ni_{0.13}Co_{0.13})O_2$ (MNC) cathode for sodium ion batteries (SIB).[120] The cathode coated with 2 ALD cycles of Al_2O_3 exhibited the best electrochemical stability and rate performance, while the one coated with 10-cycle Al_2O_3 showed the highest coulombic efficiency. The enhanced electrochemical stability may be a consequence of the protective effect and the high bandgap energy offered by the ALD Al_2O_3 coating. Furthermore, the oxide coating could provide structural stability against mechanical stresses during cycling. ALD Al_2O_3 coatings were also applied to $LiNi_{0.5}Co_{0.2}Mn_{0.3}O_2$ (NCM) particles as the cathode material for lithium ion capacitor (LIC).[121] By inhibiting the dissolution of transition metal in NCM and releasing internal stress change during cycling, the ALD Al_2O_3 coatings significantly improved the cycling capability and rate performance of the capacitor.

A method to stabilize nanostructured solid oxide fuel cell (SOFC) cathode through ALD was proposed.[122] By covering the highly active but unstable cathode $La_{0.6}Sr_{0.4}CoO_{3-\delta}$ (LSCo) with a thin ALD ZrO_2 layer, the fuel cell maintained a high oxygen reduction reactivity (ORR) at 700 °C for 4000 hours (Fig. 14). With the ALD ZrO_2 coating, the polarization area specific resistance and the degradation rate were reduced by a factor of 19 and 18 respectively. The ALD ZrO_2 coating provided the

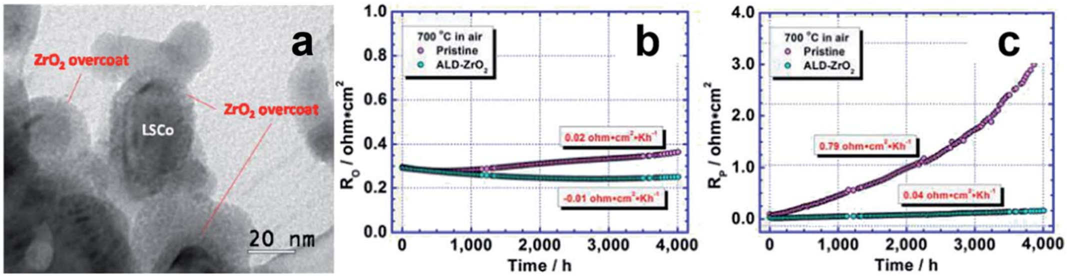

Fig. 14 (a) TEM image showing nanoscale ALD ZrO_2 coating on LSCo NPs; and comparison on long-term stability of pristine and ALD–ZrO_2 coated LSCo cathodes: (b), R_0 (overall area-specific resistance); (c), R_p (polarization area-specific resistance). Reprinted with permission from ref. 122. Copyright (2013), American Chemical Society.

porosity for O_2 to access to LSCo, conducting electrons and oxide ions, limited the thermal growth of LSCo NPs, and inhibited surface segregation of Sr.

Doping electrode particles with ions has been proved an effective way to achieve enhanced electrochemical performances. Metal ions could enter the lattice structure of cathode particles during ALD processes.[123,124] The ALD deposition process may begin at the structural defects, after the defects were saturated, the ions began to participate in the formation of oxide films on the surface of the cathode particle. Patel *et al.* reported that ALD Fe_2O_3 coating provided significant performance improvement of the LMNO cathode.[123] Compared with other doping methods, slight doping using ALD would enhance the cycle stability of LIB cathode, while excessive doping may cause distorted lattice structure or impeded Li^+ diffusion channels, which could reduce the capacity.

ALD surface modification layers have shown remarkable effects on improving the stability of cathode materials. Some results on capacity retention of ALD modified LIB cathode materials are summarized in Table 1. In order to protect the electrode material from side reactions and increase the cycle life, thicker protective coatings are preferred. Materials with limited electronic and ionic conductivity, such as alumina, may not be the best choice for cathode coating, because the increased film thickness may affect species transport and damage the capacity. Therefore, an ideal ALD coating material should be able to combine the protective effect and high electronic and ion conductivity. Accurate thickness control of the surface coating is also essential for reaching the optimal balance between high cycle life and high capacity.

3.4.2 Surface modification of anode material. Some anode materials of LIBs suffer from great capacity loss due to the formation of solid electrolyte interface (SEI) layer during the charge–discharge cycles, as well as large volume changes which may damage the anodes and expose the fresh surface. The aim of ALD modification of anode materials is to improve the battery performance by prohibiting the formation of continuous SEI layer, suppressing volume changes, and reducing side reactions.[125]

Thin films of metal oxides are preferred for anode modification. Wang *et al.* coated Al_2O_3 films onto SnO_2 anode particles by ALD.[126] They found that the ALD Al_2O_3 film with a proper thickness suppressed the volume changes of SnO_2 particles, and thus significantly improved the electrochemical behavior of the battery, especially the cycling performance. Kang *et al.* reported Fe_3O_4 nanocrystals confined in a *meso* cellular carbon foam (MSU-F-C) used as an LIB anode material.[127] An ultrathin ALD Al_2O_3 layer deposited on the composite anode could significantly improve the rate capability and durability, and reduce undesirable side reactions. Ultrathin (about 1 nm) ALD Al_2O_3 films were also coated on the surface of TiO_2 nanotubes used as the anode material.[128] Compared to the uncoated nanotube, a better electrochemical performance was achieved as a result of the increased mechanical stability and enhanced lithium ion diffusion. A composite LIB anode material was prepared by interwoven Mn_3O_4 NPs with carbon nanotube (CNT) network through a self-assembly strategy.[129] Then an ultrathin uniform ALD TiO_2 coating was deposited on the anode material to stabilize the SEI. The obtained anode material showed a high capacity, stable cycle stability, excellent rate performance, and a commercial grade area capacity. The ALD TiO_2 coating stabilized SEI provides high electronic conductivity and lithium ion diffusion ability, and improves the reaction kinetics of Mn_3O_4 through an "electron density enhancement effect".

Silicon nanostructures have shown improved capacity and cyclability in LIBs as anodes. Silicon nanowires (SiNWs) were coated with TiN films using $TiCl_4$ and NH_3 as precursors at 120 °C

Table 1 Capacity retention of ALD modified LIB cathode materials

			Capacity retention/%			
ALD material	Cathode material	Thickness/nm	Cycling number	w/o ALD	ALD	Ref.
Al_2O_3	$LiCoO_2$	0.3–0.4	120	45	89	112
TiO_2	$Li_{1.2}Ni_{0.13}Mn_{0.54}Co_{0.13}O_2$	1	100	68.2	70	114
$AlPO_4$	$Li_{1.2}Mn_{0.54}Co_{0.13}Ni_{0.13}O_2$	1	40	Drop rapidly	Stay stable	115
CeO_2	$LiMn_2O_4$	3	1000	0	62	116
CeO_2	$Li_{1.2}Mn_{0.54}Ni_{0.13}Co_{0.13}O_2$	2.5	400	22	62	118

and the coated SiNWs were used as the anode material for LIBs.[130] The conformal and uniform TiN films limited the growth of SEI and improved the mechanical stability of the anode. In addition, delamination of the nanowire assemblies from the underlying current collector were also reduced. In another work, silicon nanotubes (SiNTs) coated with ALD films of TiO_2, TiN, or Al_2O_3 on the inside, outside, or both surfaces of the nanotubes were used as the anode material for LIBs.[131] Enhanced cycling performances were obtained with almost all kinds of coatings on all surfaces. The anode material using SiNTs coated with 1.5 nm TiO_2 on both the internal and external surfaces showed the best performance.

ALD coatings have also been applied to enhance the performance of dye sensitized solar cells (DSC). In a recent work published by Li *et al.*,[132] an ultrathin TiO_2 binding layer was deposited onto TiO_2 host-particles by low temperature ALD, to enhance the interconnection between the host NPs of the photoanode, and to elevate the adhesion between the photoanode and the substrate. With the ALD coating enhanced power conversion was achieved and the ALD TiO_2 coating resulted in lower internal resistance and longer electron lifetime of the cell.

3.4.3 ALD of active electrode material. Aside from forming surface protection or modification layers, ALD are also used to deposit active materials onto conductive substrates, to produce novel electrode materials with predetermined composition, structure, and morphology. By changing these parameters, the performances of the electrode materials could be precisely tuned.

Carbon based materials are a typical class of electrode materials for their good electrical conductivity and high surface area. Construction of composite structures integrating carbon and high capacity/capacitance materials such as transition metal oxides and metal phosphates is a common strategy to take the advantages of each component and thus improve electrochemical performances.[133] A high specific capacity material $LiFePO_4$ was deposited on CNTs using a quaternary ALD process in which ferrocene ($FeCp_2$), ozone (O_3), trimethylphosphate (TMPO), water (H_2O), and lithium *t*-butoxide (LiO^tBu) were used as the precursors.[134] The surfaces of CNTs were uniformly covered with $LiFePO_4$ layers. Due to the high electric conductivity and high surface area of the CNTs, the $LiFePO_4$/CNT anode remedied the default of low rate performance of $LiFePO_4$. A high power density and ultra-long cycling lifetime were also achieved. Similarly, ultrathin Nb_2O_5 films were deposited on the surfaces of CNTs by ALD, using niobium ethoxide ($Nb(OEt)_5$) and deionized water as precursors.[135] Subsequent high temperature annealing turned the amorphous films into the hexagonal phase. The ALD Nb_2O_5@CNT anode exhibited high-rate and long-life lithium ion storage, which may be attributed to the synergistic effects of carbon nanotubes, hexagonal Nb_2O_5, and the ultrathin film structure. A novel nanostructured 3D anode material was fabricated by depositing polyimide films through MLD onto $Ti_2Nb_{10}O_{29}$ (TNO) microspheres, followed by high temperature annealing to convert the polyimide films into carbon layers.[136] The resultant TNO@C composite possessed uniformly connected conductive networks offered by MLD carbon, and the anode showed significantly improved electron/ion transport, remarkable high-rate capacity and a high capacity retention after 500 cycles of charge and discharge.

For LIB electrode materials, amorphous coatings would suppress the increasing impedance and favor lithium diffusion due to their soft structures. For instance, amorphous or crystalline ALD SnO_2 films were homogeneously deposited on both sides of graphene (GE) nanosheets to form SnO_2-GE–SnO_2 composites for LIB anodes.[137] The crystal structure of SnO_2 films could be controlled by changing the reaction conditions of ALD. Both the amorphous and crystalline SnO_2-GE anodes exhibited good electrochemical performances, but higher coulombic efficiency and better cycling stability were achieved with the amorphous SnO_2-GE anode. The buffer effect of amorphous SnO_2 could mitigate the huge volume expansion and reduce the shrinkage of SnO_2 lattice, while crystalline SnO_2 may pulverize during the charge and discharge processes.

Interstitial metal carbides have high electrical conductivity, high hardness and excellent chemical stability, which make them competitive electrode materials. An ALD assisted template synthesis strategy was reported, for the preparation of single-layer titanium carbide (TiC) hollow sphere arrays on conductive substrates.[138] In this method, polystyrene spheres (PS) were used as the template, and an ALD TiO_2 layer was uniformly coated on the PS and was then converted into TiC arrays by subsequent carbothermal reaction (Fig. 15). These TiC arrays showed exceptional long-term cycle life and excellent high-rate ability when tested as high temperature supercapacitors. Bi(1,4-di-*tert*-butyl-1,3-diazabutadienyl) nickel(II) and H_2 plasma were used to coat smooth, pure, and ideally crystallized Ni_3C films on CNTs, producing a core–shell nanostructured Ni_3C/CNT composite.[139] The ALD Ni_3C/CNT composite exhibited excellent performances as supercapacitors and for electrocatalytic hydrogen evolution.

Metal sulfides have shown great potential as the anode for LIB. For instance, the theoretical capacity of Al_2S_3 is more than 1400 mA h g^{-1}, about four times the capacity of commercial graphite anode. Aluminum sulfide (AlS_x) thin film was synthesized by ALD using tris(dimethylamido) aluminum and H_2S as precursors.[140] The ALD AlS_x film was deposited onto nitrogen-doped graphene nanosheets (NGNS) to form an anode of LIB. The anode material exhibited a high capacity of 640 mA h g^{-1} at a current density of 100 mA g^{-1} in the voltage window of 0.6–3.5 V. A reliable cyclability over 60 cycles was demonstrated.

Pt-based catalysts are widely used in the electrodes of proton exchange membrane fuel cells (PEMFCs) because of their excellent catalytic performances in both hydrogen oxidation and oxygen reduction reactions (ORR). However, conventional Pt/C catalysts exhibit poor durability due to the detachment and agglomeration of Pt NPs during fuel cell operation. Lee *et al.* reported a method of synthesizing high-performance Pt/carbon catalyst for PEMFCs using FBR ALD.[141] Two types of carbon supports were tested. Uniformly dispersed and highly dense Pt NPs obtained by ALD with an optimized ionomer content exhibited high fuel cell performance and excellent stability. WN was deposited on the ALD Pt/C catalyst using bis(*tert*-butylimido)bis(dimethylamido) tungsten and ammonia as precursors, producing a conformal coating on the surface of the catalyst particles.[142] The subsequent thermal treatment led to a reduced amount of nitride and separated Pt and W domains.

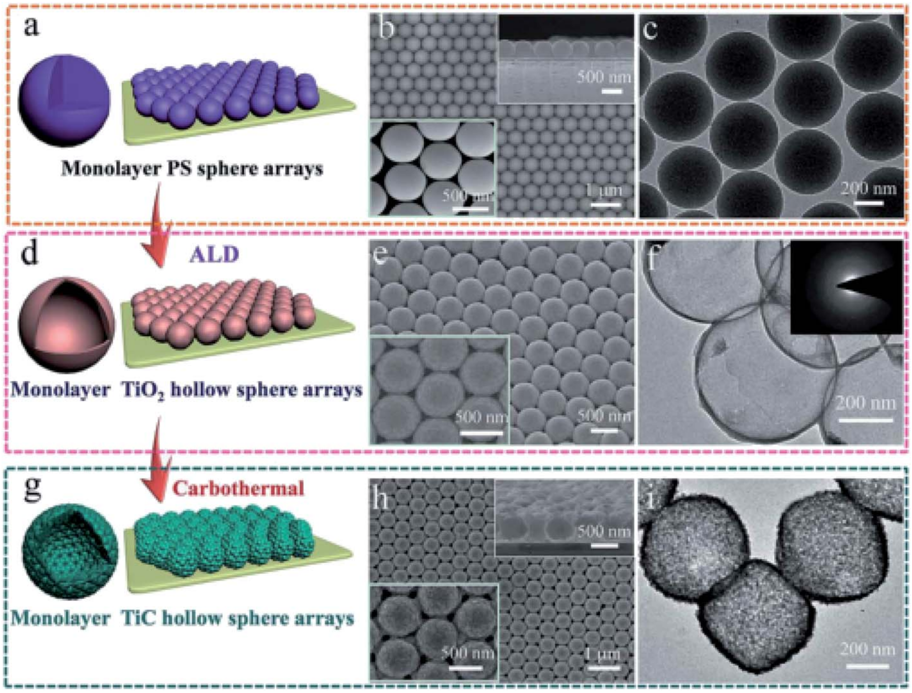

Fig. 15 (a, d and g) Fabrication process of monolayer TiC hollow sphere arrays on a graphite paper substrate; (b and c), SEM and TEM images of the PS sphere template; (e and f), SEM and TEM images of the TiO_2 hollow sphere arrays; (h and i), SEM and TEM images of the TiC hollow sphere arrays. Reprinted with permission from ref. 138. Copyright (2013), Royal Society of Chemistry.

The surface modified Pt/C catalyst showed an ORR activity (465 mA mg^{-1}) much higher than that of the bare Pt/C catalyst (277 mA mg^{-1}). After accelerated durability test, the surface modified catalyst exhibited better retention of electrochemical properties and higher mechanical stability. A porous organic–inorganic hybrid inter-layer was deposited on a CNT support through MLD using sequential exposures of TMA and glycerol at 150 °C, followed by high temperature annealing.[143] Pt NPs were subsequently deposited onto the MLD-modified CNT surface by ALD. The MLD-modified CNT surface with enriched pores helped anchoring the Pt species and avoided agglomeration or detachment of the NPs. Besides, the inter-layer induced electron transfer from Pt to the substrate. Therefore the as-prepared Pt catalysts showed significantly enhanced ORR activity and durability compared to the catalysts grown on the bare CNT.

3.5 Wave absorbing material

In recent years, wave-absorbing materials are more and more widely used in military and civilian fields. The common wave absorbing agents are powders of carbonyl iron, ferrite, barium titanite, and so on. Carbonyl iron powder has high magnetic permeability, good absorbing ability, and wide absorbing frequency bandwidth, therefore it has become one of the most widely used absorbing materials. However, corrosion and oxidation limit its applications under certain conditions. To improve the corrosion resistance and electromagnetic performance of carbonyl iron, Al_2O_3 thin films were coated on the carbonyl iron powder by ALD.[144] The ALD Al_2O_3 films conformally covered the surfaces of carbonyl iron particles. Thermal stability and corrosion resistance of the surface modified carbonyl iron powder were significantly improved. Besides, electromagnetic parameters and wave absorbing properties were also enhanced. Under the same experiment conditions, a 40.9% lower reflection loss (RL) can be obtained.

For practical application of microwave absorbing materials (MAMs), effective electromagnetic (EM) impedance matching between the permeability and the relative permittivity is crucial to achieve strong absorption. An efficient and lightweight EM absorbing material was prepared by Wang *et al.* through mixing ALD Fe_3O_4/graphene and Ni/graphene composites. The ALD Fe_3O_4 and Ni NPs had narrow size distributions, and were uniformly dispersed throughout the entire graphene surface. The minimum optical reflection loss was −46.4 dB at 15.6 GHz, with a coating thickness of only 1.4 mm. The promoted EM absorption property of the composite material was ascribed to the effective impedance matching, multiple interfacial polarization and increased magnetic loss from the added magnetic constituents.[145] The same group also proposed a method to produce ZnO supported Ni NPs with enhanced microwave absorption.[146] NiO films were uniformly deposited on ZnO particles by ALD, followed by high temperature reduction to synthesize flower-like ZnO coated with Ni NPs. The ZnO@Ni composite exhibited significantly improved EM absorption properties compared to ZnO (Fig. 16). The enhanced absorption capacity was explained by the combination of various dielectric–magnetic loss mechanisms.

A new type of microwave absorbing material was synthesized by coating carbon nanofibers with multilayer gradient films through ALD.[147] The gradient nanofilm was composed of ZnO with different Al_2O_3 content, which was prepared by alternating ALD ZnO and ALD Al_2O_3 cycles at different ratios. The

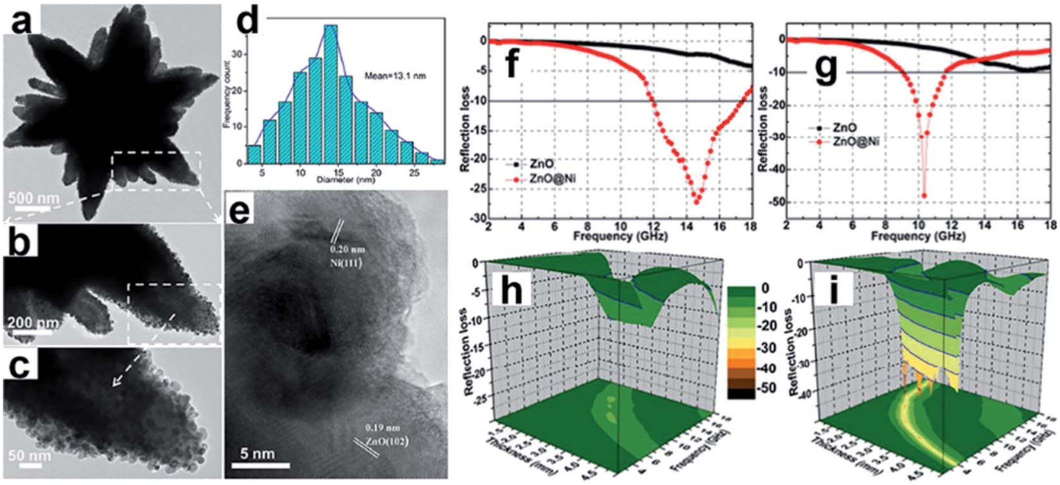

Fig. 16 (a–c) TEM images of ZnO@Ni; (d), size distribution of Ni NPs; (e), HRTEM image of ZnO@Ni; RL curves of ZnO@Ni composites with a thickness of 1.5 mm (f) and 2 mm (g); 3D representations of RL of ZnO (h) and ZnO@Ni. (i) Reprinted with permission from ref. 146. Copyright (2013), Royal Society of Chemistry.

multilayer gradient film acted as intermediate layers to tune the impedance matching between air and the nanofiber surface, and the microwave absorption performance was remarkably enhanced. A reflection loss of −58.5 dB was achieved at 16.2 GHz with a composite thickness of only 1.8 mm. In Table 2, the wave absorption performances of different materials fabricated by ALD are listed and compared.

3.6 Medicine

There is a great demand for surface modification and engineering in the medical field. Through proper surface modification, the following goals may be achieved: protection and stabilization of pharmaceutical ingredients; controlled release of drugs; enhanced penetration of medicine into human tissues; improved biocompatibility of surgical devices, implants, and artificial tissues.[148] ALD perfectly meet the needs of surface engineering in the medical field, and many opportunities are related to powder fabrication.

Active pharmaceutical ingredients (APIs) are mainly organic solid powders. In order to be prepared in a variety of dosage forms, many APIs require processing. Powder flow improvement and APIs protection are often desirable. Due to the inhomogeneous nature and irregular shapes of drug particles, conventional coating techniques can hardly achieve conformal coating around the particles. ALD is a potential way to encapsulate drug particles with high quality coatings. Micrometer scale acetaminophen particles were coated with ALD Al_2O_3, TiO_2 and ZnO in a rotary reactor.[149] The main polymorph remained unchanged during the ALD process. HPLC analysis showed that no degradation product was produced, which confirmed the stability of ALD coated drug samples. ALD metal oxide coated acetaminophen showed slowed drug release. ALD Al_2O_3 and TiO_2 coated acetaminophen particles exhibited good cytocompatibility. Evaluation *in vitro* on intestinal Caco-2 cells indicated that thick ZnO coatings showed the greatest cytotoxicity among the materials studied.

ALD coatings were also used for improving the stability of drug particles. Hellrup *et al.*[150] investigated the feasibility of applying ALD Al_2O_3 coatings to prevent moisture absorption. Dynamic moisture absorption experiments showed that the ALD Al_2O_3 nanoshells almost completely inhibited the adsorption of water. These results have demonstrated the potential of ALD coatings in improving the long-term stability of drug particles.

Vitamin C is a very important and commonly used medicine, but it suffers from rapid oxidation/degradation in light and humidity. Haghshenas-Lari *et al.* applied TiO_2 coatings to protect the surface of vitamin C particles by ALD, and studied the effects of ALD experiment parameters on the structure and quality of TiO_2 coating.[151] It was demonstrated that the ALD TiO_2 coating can successfully slow down the degradation and improve the medical stability of vitamin C.

Table 2 Wave absorption properties of different materials fabricated by ALD

		Frequency for RL ≤ −10 dB/GHz			RL min/dB			
ALD material	Original wave absorbing material	Thickness/mm	w/o ALD	ALD	Thickness/mm	w/o ALD	ALD	Ref.
Al_2O_3	Carbonyl iron powder	2.5	2.42–3.87	2.76–4.65	2.5	−14.5	−20.3	144
Fe_3O_4	Graphene	1.5	—	12.4–16.9	1.4	−3.3	−46.4	145
Ni	Flower-like ZnO	1.5	—	12.1–17.4	2	−9.3	−48	146
ZnO/Al_2O_3	Carbon nanofibers	1.9	—	12.7–18	1.8	−9.2	−58.5	147

ALD protective coatings can also be applied to enhance the medical stability of vaccine.[152] Affected by its instability, vaccines usually require refrigerated storage and multiple vaccinations, and thus the practical impacts of the vaccine are often compromised. Garcea *et al.* prepared thermostabilized powders containing HPV16L1 ingredient using spray drying, and coated these powders with ALD alumina layers to protect the inside antigens and modulate the release. With the ALD alumina protective coating, the antibody titers were unaffected by incubation at 50 °C for one month. Antibody response test demonstrated that a single dose of the ALD-coated vaccine produced neutralizing responses and antibody titers were equivalent or superior to conventional alum-adsorbed two-dose immunization of the L1 protein.

Zhang *et al.* reported ALD modification of budesonide and lactose organic particles with atomic scale Al_2O_3 films.[153] A vibration-assisted fluidized bed ALD reactor was used, and the coating experiments were carried out under near ambient conditions (<40 °C, 1 bar). Complete and conformal coating on the drug particles (Fig. 17a) and the feasibility to tailor heat transfer, dissolution rate and dispersibility were demonstrated. With the increasing ALD Al_2O_3 film thickness, the dissolution rates of both budesonide and lactose particles were reduced, which indicated the potential application of ALD coatings for controlled drug release. The coated drug powders were less cohesive, which implied improved powder processability after the ALD surface modification.

Hellrup *et al.* also performed pharmacokinetic studies showing that ALD Al_2O_3 nanoshells coated on the APIs can be used to achieve long sustained drug release.[154] 30 nm-thick ALD Al_2O_3 coating was deposited onto micro particles of indomethacin, and the drug level in blood samples were tested in rats for 12 weeks (Fig. 17b). The uncoated indomethacin was eliminated with a half-life of 15 h, and the coated samples showed dramatically slower release rate which sustained for more than 12 weeks.

4. Conclusion and perspective

The growing demands for controllable surface modification of powder materials and precise manufacture of nanostructures have stimulated the development of ALD technology for powder fabrication. This article starts with a brief introduction to the principles of ALD, followed by a retrospection on the development of ALD reactors designed for powder fabrication, and then illustrates typical examples of applications of ALD for

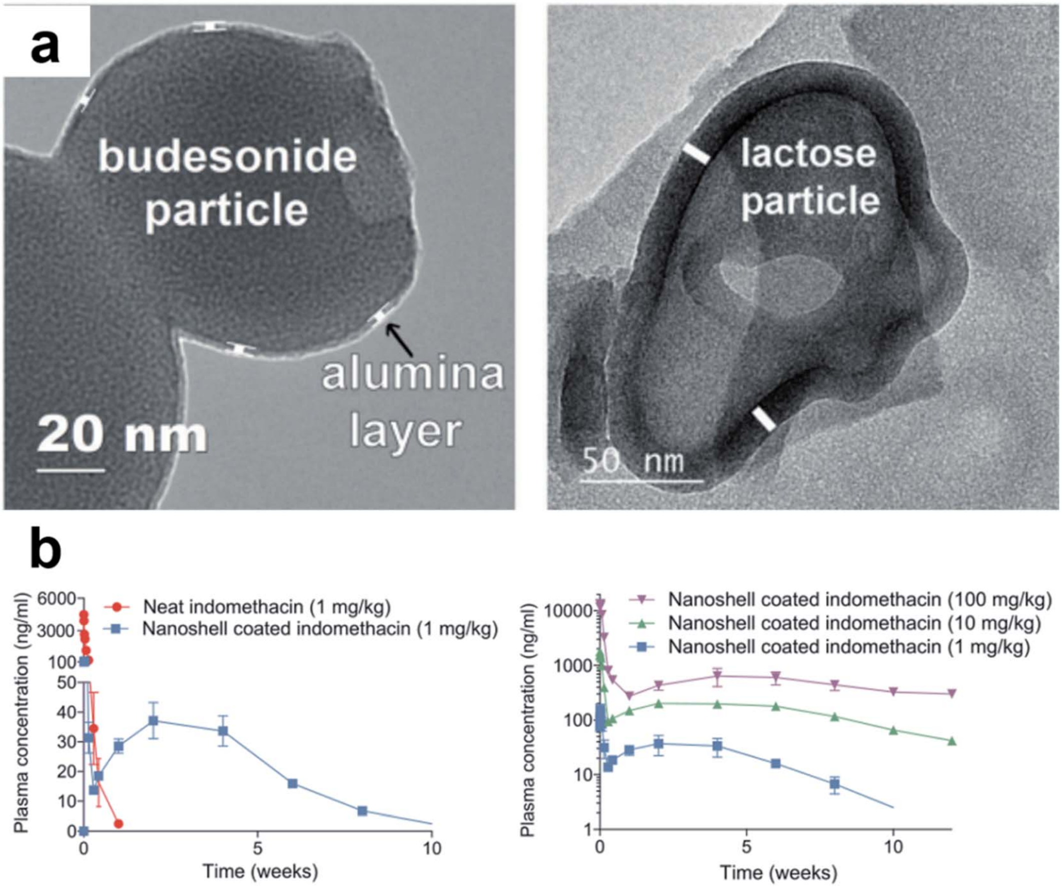

Fig. 17 (a) TEM images of ALD Al_2O_3 coated budesonide (left) and lactose (right) particles; Reprinted with permission from ref. 153. Copyright (2017), Royal Society of Chemistry. (b) Plasma concentration curves for indomethacin measured on blood samples from test animals at different times. Reprinted from ref. 154. Copyright (2019), with permission from Elsevier.

fabricating powder materials in various fields. The advantages of ALD for powder fabrication include the diversity of selectable ALD and substrate materials; the conformality of the produced films on 3D structures; the uniformity and high dispersion of the obtained discontinuous structures; and most importantly, the ability to precisely control the dimension as a result of the self-limiting ALD surface reaction. These features make ALD a very unique and effective tool for powder fabrication.

The strong potential of ALD for powder fabrication has been proved in many areas, and ALD technology may be applied to even more areas in the future, to produce novel materials or structures through precise surface engineering of powders. For existing applications, ALD powder fabrication may move towards the goal of mass production and cost reduction. Whereas there are still many problems that need to be solved:

(1) The research on ALD reactors and processes for industrial scale powder fabrication should be advanced. Existing fluidized bed reactors, rotating reactors and spatial reactors have demonstrated the potential for mass production of powder materials. The existing reactor designs need to be improved and new reactor designs should be investigated to enhance the mass and heat transfer, reduce the particle agglomeration, and increase the utilization of precursors.

(2) The development of economical precursors and corresponding surface reactions are also necessary for the large scale application of ALD, especially for scalable fabrication of powder materials with huge surface areas.

(3) Emerging applications of ALD powder fabrication should be further investigated. More surface modification/functionalization materials should be tested and novel structures should be designed and synthesized to optimize their performances. Evaluation on the merit or importance of the technology (for instance, significance in improving scientific understanding or potential for industrial application) should be made.

The potential applications for ALD are virtually endless. Surface engineering of powder materials at atomic level precision will enable introduction of the desired structural, physical, or chemical properties to the surface of the powder, which will significantly enrich and promote the performances and/or functions of the materials. The future research of ALD for powder material fabrication may be full of challenges, but it is certainly rewarding.

Abbreviates

AC	Activated carbon
ALD	Atomic layer deposition
AP	Ammonium perchlorate
APH	Aqueous-phase hydrogenation
APIs	Active pharmaceutical ingredients
CNT	Carbon nanotubes
CVD	Chemical vapor deposition
DEZ	Diethyl zinc
DFT	Density functional theory
DRM	Dry reforming of methane
DSC	Dye sensitized solar cells
DTA	Differential thermal analysis
EBC	Environmental barrier coating
EM	Effective electromagnetic
ESD	Electrostatic discharge
EXAFS	Extended X-ray absorption fine structure
FBRs	Fluidized bed reactors
FTIR	Fourier transform infrared
GE	Graphene
GISAXS	Grazing incidence small-angle X-ray scattering
HAADF-STEM	High angle annular dark field scanning transmission electron microscopy
HER	Hydrogen evolution reaction
LIB	Lithium-ion batteries
LIC	Lithium-ion capacitors
MAMs	Microwave absorbing materials
MLD	Molecular layer deposition
MO	Metal oxide
MOFs	Metal organic frameworks
NMR	Nuclear magnetic resonance
NPs	Nanoparticles
NTs	Nanotubes
NWs	Nanowires
ODH	Oxidative dehydrogenation
OER	Oxygen evolution reaction
ORR	Oxygen reduction reaction
PEMFCs	Proton exchange membrane fuel cells
PS	Polystyrene spheres
PS-DVB	Poly styrene-divinylbenzene
rGO	Reduced graphene oxide
SAMS	Self-assembled monolayers
SEI	Solid electrolyte interphase
SEM	Scanning electron microscope
SERS	Surface enhanced Raman scattering
SIB	Sodium ion batteries
SOFC	Solid oxide fuel cells
TEM	Transmission electron microscope
TMA	Trimethyl aluminum
WGS	Water-gas shift
XAFS	X-ray absorption fine structure spectroscopy
XANES	X-ray absorption near edge structure
XRD	X-ray diffraction
XRF	X-ray fluorescence

Conflicts of interest

There are no conflicts to declare.

Acknowledgements

This work is financially supported by National Science Foundation of China (grant number: 21975200).

References

1 S. Adhikari, S. Selvaraj and D.-H. Kim, *Adv. Mater. Interfaces*, 2018, **5**, 1800581.
2 S. M. George, *Chem. Rev.*, 2010, **110**, 111–131.

3 D. M. King, X. H. Liang and A. W. Weimer, *Powder Technol.*, 2012, **221**, 13–25.

4 C. Marichy, M. Bechelany and N. Pinna, *Adv. Mater.*, 2012, **24**, 1017–1032.

5 M. Leskelä and M. Ritala, *Thin Solid Films*, 2002, **409**, 138–146.

6 R. W. Johnson, A. Hultqvist and S. F. Bent, *Mater. Today*, 2014, **17**, 236–246.

7 A. W. Weimer, *J. Nanopart. Res.*, 2019, **21**, 42.

8 T. Suntola, *Mater. Sci. Rep.*, 1985, **4**, 261–312.

9 J. D. Ferguson, A. W. Weimer and S. M. George, *Thin Solid Films*, 2000, **371**, 95–104.

10 J. Libera, J. Elam and M. Pellin, *Thin Solid Films*, 2008, **516**, 6158–6166.

11 J. R. Wank, S. M. George and A. W. Weimer, *Powder Technol.*, 2001, **121**, 195–204.

12 J. R. Wank, S. M. George and A. W. Weimer, *J. Am. Ceram. Soc.*, 2004, **87**, 762–765.

13 J. R. Wank, S. M. George and A. W. Weimer, *Powder Technol.*, 2004, **142**, 59–69.

14 D. M. King, J. A. Spencer, X. Liang, L. F. Hakim and A. W. Weimer, *Surf. Coat. Technol.*, 2007, **201**, 9163–9171.

15 L. F. Hakim, J. L. Portman, M. D. Casper and A. W. Weimer, *Powder Technol.*, 2005, **160**, 149–160.

16 R. Beetstra, U. Lafont, J. Nijenhuis, E. M. Kelder and J. R. van Ommen, *Chem. Vap. Deposition*, 2009, **15**, 227–233.

17 H. Van Bui, F. Grillo, R. Helmer, A. Goulas and J. R. van Ommen, *J. Phys. Chem. C*, 2016, **120**, 8832–8840.

18 H. Tiznado, D. Domínguez, F. Muñoz-Muñoz, J. Romo-Herrera, R. Machorro, O. E. Contreras and G. Soto, *Powder Technol.*, 2014, **267**, 201–207.

19 J. A. McCormick, B. L. Cloutier, A. W. Weimer and S. M. George, *J. Vac. Sci. Technol., A*, 2007, **25**, 67–74.

20 C. L. Duan, X. Liu, B. Shan and R. Chen, *Rev. Sci. Instrum.*, 2015, **86**, 3727.

21 P. Poodt, A. Lankhorst, F. Roozeboom, K. Spee, D. Maas and A. Vermeer, *Adv. Mater.*, 2010, **22**, 3564–3567.

22 P. Poodt, D. C. Cameron, E. Dickey, S. M. George, V. Kuznetsov, G. N. Parsons, F. Roozeboom, G. Sundaram and A. Vermeer, *J. Vac. Sci. Technol., A*, 2012, **30**, 11.

23 J. R. van Ommen, D. Kooijman, M. de Niet, M. Talebi and A. Goulas, *J. Vac. Sci. Technol., A*, 2015, **33**, 5.

24 C. L. Duan, Z. Deng, K. Cao, H. F. Yin, B. Shan and R. Chen, *J. Vac. Sci. Technol., A*, 2016, **34**, 8.

25 V. Cremers, G. Rampelberg, A. Barhoum, P. Walters, N. Claes, T. M. de Oliveira, G. Van Assche, S. Bals, J. Dendooven and C. Detavernier, *Surf. Coat. Technol.*, 2018, **349**, 1032–1041.

26 A. L. Hoskins, A. H. Coffey, C. B. Musgrave and A. W. Weimer, *J. Am. Ceram. Soc.*, 2018, **101**, 2493–2505.

27 H. Azizpour, M. Talebi, F. D. Tichelaar, R. Sotudeh-Gharebagh, J. Guo, J. R. van Ommen and N. Mostoufi, *Appl. Surf. Sci.*, 2017, **426**, 480–496.

28 X. Liang and A. W. Weimer, *J. Nanopart. Res.*, 2010, **12**, 135–142.

29 D. M. King, X. H. Liang, B. B. Burton, M. K. Akhtar and A. W. Weimer, *Nanotechnology*, 2008, **19**, 8.

30 J. Guo, H. V. Bui, D. Valdesueiro, S. J. Yuan, B. Liang and J. R. van Ommen, *Nanomaterials*, 2018, **8**, 19.

31 R. Verstraete, G. Rampelberg, H. Rijckaert, I. Van Driessche, E. Coetsee, M. M. Duvenhage, P. F. Smet, C. Detavernier, H. Swart and D. Poelman, *Chem. Mater.*, 2019, **31**, 7192–7202.

32 E. Karacaoglu, E. Ozturk, M. Uyaner and M. D. Losego, *J. Am. Ceram. Soc.*, 2020, **103**, 3706–3715.

33 S. Bhattacharya, L. Jamison, D. N. Seidman, W. Mohamed, Y. Bei, M. J. Pellin and A. M. Yacout, *J. Nucl. Mater.*, 2019, **526**, 9.

34 S. L. Zhang, E. Yu, S. Gates, W. S. Cassata, J. Makel, A. M. Thron, C. Bartel, A. W. Weimer, R. Faller, P. Stroeve and J. W. Tringe, *J. Nucl. Mater.*, 2018, **499**, 301–311.

35 S. K. Bull, W. W. McNeary, C. A. Adkins, T. A. Champ, C. A. Hill, R. C. O'Brien, C. B. Musgrave and A. W. Weimer, *Appl. Surf. Sci.*, 2020, **507**, 9.

36 B. J. O'Neill, D. H. K. Jackson, J. Lee, C. Canlas, P. C. Stair, C. L. Marshall, J. W. Elam, T. F. Kuech, J. A. Dumesic and G. W. Huber, *ACS Catal.*, 2015, **5**, 1804–1825.

37 R. L. Puurunen and W. Vandervorst, *J. Appl. Phys.*, 2004, **96**, 7686–7695.

38 J. Hämäläinen, M. Ritala and M. Leskelä, *Chem. Mater.*, 2014, **26**, 786–801.

39 H. Feng, J. W. Elam, J. A. Libera, W. Setthapun and P. C. Stair, *Chem. Mater.*, 2010, **22**, 3133–3142.

40 H. Feng, J. A. Libera, P. C. Stair, J. T. Miller and J. W. Elam, *ACS Catal.*, 2011, **1**, 665–673.

41 T. Gong, L. Qin, W. Zhang, H. Wan, J. Lu and H. Feng, *J. Phys. Chem. C*, 2015, **119**, 11544–11556.

42 W. Zhang, Y. Huang, T. Gong and H. Feng, *Catal. Commun.*, 2017, **93**, 47–52.

43 T. Gong, Y. Huang, L. J. Qin, W. L. Zhang, J. G. Li, L. F. Hui and H. Feng, *Appl. Surf. Sci.*, 2019, **495**, 12.

44 M. Lashdaf, J. Lahtinen, M. Lindblad, T. Venäläinen and A. O. I. Krause, *Appl. Catal., A*, 2004, **276**, 129–137.

45 A. Goulas and J. R. van Ommen, *J. Mater. Chem. A*, 2013, **1**, 4647–4650.

46 J. K. Zhang, C. Q. Chen, S. Chen, Q. M. Hu, Z. Gao, Y. Q. Li and Y. Qin, *Catal. Sci. Technol.*, 2017, **7**, 322–329.

47 J. Dendooven, R. K. Ramachandran, E. Solano, M. Kurttepeli, L. Geerts, G. Heremans, J. Ronge, M. M. Minjauw, T. Dobbelaere, K. Devloo-Casier, J. A. Martens, A. Vantomme, S. Bals, G. Portale, A. Coati and C. Detavernier, *Nat. Commun.*, 2017, **8**, 12.

48 K. Leus, J. Dendooven, N. Tahir, R. K. Ramachandran, M. Meledina, S. Turner, G. Van Tendeloo, J. L. Goeman, J. Van der Eycken, C. Detavernier and P. Van Der Voort, *Nanomaterials*, 2016, **6**, 11.

49 B. Qiao, A. Wang, X. Yang, L. F. Allard, Z. Jiang, Y. Cui, J. Liu, J. Li and T. Zhang, *Nat. Chem.*, 2011, **3**, 634.

50 S. H. Sun, G. X. Zhang, N. Gauquelin, N. Chen, J. G. Zhou, S. L. Yang, W. F. Chen, X. B. Meng, D. S. Geng, M. N. Banis, R. Y. Li, S. Y. Ye, S. Knights, G. A. Botton, T. K. Sham and X. L. Sun, *Sci. Rep.*, 2013, **3**, 9.

51 N. C. Cheng, S. Stambula, D. Wang, M. N. Banis, J. Liu, A. Riese, B. W. Xiao, R. Y. Li, T. K. Sham, L. M. Liu, G. A. Botton and X. L. Sun, *Nat. Commun.*, 2016, **7**, 9.

52 Z. X. Song, Y. N. Zhu, H. S. Liu, M. N. Banis, L. Zhang, J. J. Li, K. Doyle-Davis, R. Y. Li, T. K. Sham, L. J. Yang, A. Young, G. A. Botton, L. M. Liu and X. L. Sun, *Small*, 2020, **16**, 12.

53 K. Ding, A. Gulec, A. M. Johnson, N. M. Schweitzer, G. D. Stucky, L. D. Marks and P. C. Stair, *Science*, 2015, **350**, 189–192.

54 H. Yan, Y. Lin, H. Wu, W. Zhang, Z. Sun, H. Cheng, W. Liu, C. Wang, J. Li and X. Huang, *Nat. Commun.*, 2017, **8**, 1–11.

55 H. Yan, H. Cheng, H. Yi, Y. Lin, T. Yao, C. Wang, J. Li, S. Wei and J. Lu, *J. Am. Chem. Soc.*, 2015, **137**, 10484–10487.

56 X. H. Huang, Y. J. Xia, Y. J. Cao, X. S. Zheng, H. B. Pan, J. F. Zhu, C. Ma, H. W. Wang, J. J. Li, R. You, S. Q. Wei, W. X. Huang and J. L. Lu, *Nano Res.*, 2017, **10**, 1302–1312.

57 Z. Y. Shang, S. G. Li, L. Li, G. Z. Liu and X. H. Liang, *Appl. Catal., B*, 2017, **201**, 302–309.

58 C. S. Chen, J. H. Lin, T. W. Lai and B. H. Li, *J. Catal.*, 2009, **263**, 155–166.

59 X. Liang, N.-H. Li and A. W. Weimer, *Microporous Mesoporous Mater.*, 2012, **149**, 106–110.

60 H. Feng, J. W. Elam, J. A. Libera, M. J. Pellin and P. C. Stair, *J. Catal.*, 2010, **269**, 421–431.

61 G.-Q. Yang, H. Wang, T. Gong, Y.-H. Song, H. Feng, H.-Q. Ge, H.-b. Ge, Z.-T. Liu and Z.-W. Liu, *J. Catal.*, 2019, **380**, 195–203.

62 M. G. Jeong, E. J. Park, B. Jeong, D. H. Kim and Y. D. Kim, *Chem. Eng. J.*, 2014, **237**, 62–69.

63 X. L. Tong, Y. Qin, X. Y. Guo, O. Moutanabbir, X. Y. Ao, E. Pippel, L. B. Zhang and M. Knez, *Small*, 2012, **8**, 3390–3395.

64 R. Singh, R. Bapat, L. Qin, H. Feng and V. Polshettiwar, *ACS Catal.*, 2016, **6**, 2770–2784.

65 C. Q. Chen, P. Li, G. Z. Wang, Y. Yu, F. F. Duan, C. Y. Chen, W. G. Song, Y. Qin and M. Knez, *Angew. Chem., Int. Ed.*, 2013, **52**, 9196–9200.

66 A. Podurets, D. Kolokolov, M. K. S. Barr, E. Ubyivovk, M. Osmolowsky, N. Bobrysheva, J. Bachmann and O. Osmolovskaya, *Appl. Surf. Sci.*, 2020, **533**, 9.

67 T. Gong, L. Qin, J. Lu and H. Feng, *Phys. Chem. Chem. Phys.*, 2016, **18**, 601–614.

68 N. Yan, L. Qin, J. Li, F. Zhao and H. Feng, *Appl. Surf. Sci.*, 2018, **451**, 155–161.

69 C. Q. Chen, F. F. Duan, S. C. Zhao, W. K. Wang, F. Yang, W. Nuansing, B. Y. Zhang, Y. Qin and M. Knez, *Appl. Catal., B*, 2019, **248**, 218–225.

70 N. P. Dasgupta, X. B. Meng, J. W. Elam and A. B. F. Martinson, *Acc. Chem. Res.*, 2015, **48**, 341–348.

71 A. W. Peters, Z. Li, O. K. Farha and J. T. Hupp, *ACS Nano*, 2015, **9**(8), 8484–8490.

72 H. Li, Y. D. Shao, Y. T. Su, Y. H. Gao and X. W. Wang, *Chem. Mater.*, 2016, **28**, 1155–1164.

73 H. Choi, A. W. Peters, H. Noh, L. C. Gallington, A. E. Platero-Prats, M. R. DeStefano, M. Rimoldi, S. Goswami, K. W. Chapman, O. K. Farha and J. T. Hupp, *ACS Appl. Energy Mater.*, 2019, **2**, 8695–8700.

74 Z. Y. He, Z. Guo, Q. B. Wa, X. Zhong, X. W. Wang and Y. Chen, *J. Mater. Res.*, 2020, **35**, 822–830.

75 H. Li, R. Zhao, J. H. Zhu, Z. Guo, W. Xiong and X. W. Wang, *Chem. Mater.*, 2020, **32**, 8885–8894.

76 J. Lu, J. W. Elam and P. C. Stair, *Surf. Sci. Rep.*, 2016, **71**, 410–472.

77 S. T. Christensen, F. Hao, J. L. Libera, N. Guo, J. T. Miller, P. C. Stair and J. W. Elam, *Nano Lett.*, 2010, **10**, 3047.

78 K. Cao, Q. Q. Zhu, B. Shan and R. Chen, *Sci. Rep.*, 2015, **5**, 7.

79 J. L. Lu, K. B. Low, Y. Lei, J. A. Libera, A. Nicholls, P. C. Stair and J. W. Elam, *Nat. Commun.*, 2014, **5**, 9.

80 H. Wang, C. Wang, H. Yan, H. Yi and J. Lu, *J. Catal.*, 2015, **324**, 59–68.

81 J. L. Lu, B. S. Fu, M. C. Kung, G. M. Xiao, J. W. Elam, H. H. Kung and P. C. Stair, *Science*, 2012, **335**, 1205–1208.

82 H. M. Duan, R. You, S. T. Xu, Z. R. Li, K. Qian, T. Cao, W. X. Huang and X. H. Bao, *Angew. Chem., Int. Ed.*, 2019, **58**, 12043–12048.

83 H. Feng, J. L. Lu, P. C. Stair and J. W. Elam, *Catal. Lett.*, 2011, **141**, 512–517.

84 H. B. Zhang, X. K. Gu, C. Canlas, A. J. Kropf, P. Aich, J. P. Greeley, J. W. Elam, R. J. Meyers, J. A. Dumesic, P. C. Stair and C. L. Marshall, *Angew. Chem., Int. Ed.*, 2014, **53**, 12132–12136.

85 H. Yi, H. Y. Du, Y. L. Hu, H. Yan, H. L. Jiang and J. L. Lu, *ACS Catal.*, 2015, **5**, 2735–2739.

86 J. F. Yang, K. Cao, M. Gong, B. Shan and R. Chen, *J. Catal.*, 2020, **386**, 60–69.

87 E. Solano, J. Dendooven, J. Y. Feng, P. Bruner, M. M. Minjauw, R. K. Ramachandran, M. Van Daele, K. Van de Kerckhove, T. Dobbelaere, A. Coati, D. Hermida-Merino and C. Detavernier, *Nanoscale*, 2020, **12**, 11684–11693.

88 J. M. Cai, J. Zhang, K. Cao, M. Gong, Y. Lang, X. Liu, S. Q. Chu, B. Shan and R. Chen, *ACS Appl. Nano Mater.*, 2018, **1**, 522–530.

89 Q. Yao, C. L. Wang, H. W. Wang, H. Yan and J. L. Lu, *J. Phys. Chem. C*, 2016, **120**, 9174–9183.

90 B. J. O'Neill, D. H. K. Jackson, A. J. Crisci, C. A. Farberow, F. Shi, A. C. Alba-Rubio, J. Lu, P. J. Dietrich, X. Gu, C. L. Marshall, P. C. Stair, J. W. Elam, J. T. Miller, F. H. Ribeiro, P. M. Voyles, J. Greeley, M. Mavrikakis, S. L. Scott, T. F. Kuech and J. A. Dumesic, *Angew. Chem., Int. Ed.*, 2013, **52**, 13808–13812.

91 H. B. Zhang, Y. Lei, A. J. Kropf, G. H. Zhang, J. W. Elam, J. T. Miller, F. Sollberger, F. Ribeiro, M. C. Akatay, E. A. Stach, J. A. Dumesic and C. L. Marshall, *J. Catal.*, 2014, **317**, 284–292.

92 H. B. Zhang, C. Canlas, A. J. Kropf, J. W. Elam, J. A. Dumesic and C. L. Marshall, *J. Catal.*, 2015, **326**, 172–181.

93 J. C. Lee, D. H. K. Jackson, T. Li, R. E. Winans, J. A. Dumesic, T. F. Kuech and G. W. Huber, *Energy Environ. Sci.*, 2014, **7**, 1657–1660.

94 Y. Zhou, D. M. King, J. H. Li, K. S. Barrett, R. B. Goldfarb and A. W. Weimer, *Ind. Eng. Chem. Res.*, 2010, **49**, 6964–6971.

95 R. Kumar, P. F. Siril and P. Soni, *Def. Technol.*, 2015, **11**, 382–389.

96 D. Wen, *Energy Environ. Sci.*, 2010, **3**, 591.

97 J. D. Ferguson, K. J. Buechler, A. W. Weimer and S. M. George, *Powder Technol.*, 2005, **156**, 154–163.

98 L. Qin, T. Gong, H. Hao, K. Wang and H. Feng, *J. Nanopart. Res.*, 2013, **15**, 2150.

99 L. Qin, N. Yan, J. Li, H. Hao, F. Zhao and H. Feng, *RSC Adv.*, 2017, **7**, 7188–7197.

100 N. Yan, L. J. Qin, H. X. Hao, L. F. Hui, F. Q. Zhao and H. Feng, *Appl. Surf. Sci.*, 2017, **408**, 51–59.

101 R. Chen, C.-L. Duan, X. Liu, K. Qu, G. Tang, X.-X. Xu and B. Shan, *J. Vac. Sci. Technol., A*, 2017, **35**, 03E111.

102 R. Chen, K. Qu, J. Li, P. Zhu, C. Duan, J. Zhang, X. Li, X. Liu and Z. Yang, *ACS Appl. Nano Mater.*, 2018, **1**, 5500–5506.

103 L. Qin, Y. Ning, H. Hao, T. An, F. Zhao and F. Hao, *Appl. Surf. Sci.*, 2018, **436**, 548–555.

104 L. J. Qin, T. Gong, J. G. Li, N. Yan, L. F. Hui and H. Feng, *J. Hazard. Mater.*, 2019, **378**, 8.

105 B. Scrosati and J. Garche, *J. Power Sources*, 2010, **195**, 2419–2430.

106 X. B. Meng, X. Q. Yang and X. L. Sun, *Adv. Mater.*, 2012, **24**, 3589–3615.

107 C. Guan and J. Wang, *Adv. Sci.*, 2016, **3**, 23.

108 M. Lu, R. B. Nuwayhid, T. Wu, L. Yu and J. Lu, *Adv. Mater. Interfaces*, 2016, **3**, 1600564.

109 H. C. M. Knoops, M. E. Donders, M. C. M. van de Sanden, P. H. L. Notten and W. M. M. Kessels, *J. Vac. Sci. Technol., A*, 2012, **30**, 010801.

110 B. Ahmed, C. Xia and H. N. Alshareef, *Nano Today*, 2016, **11**, 250–271.

111 B. Yan, X. F. Li, Z. M. Bai, X. S. Song, D. B. Xiong, M. L. Zhao, D. J. Li and S. G. Lu, *J. Power Sources*, 2017, **338**, 34–48.

112 Y. S. Jung, A. S. Cavanagh, A. C. Dillon, M. D. Groner, S. M. George and S.-H. Lee, *J. Electrochem. Soc.*, 2010, **157**, A75–A81.

113 X. F. Li, J. Liu, X. B. Meng, Y. J. Tang, M. N. Banis, J. L. Yang, Y. H. Hu, R. Y. Li, M. Cai and X. L. Sun, *J. Power Sources*, 2014, **247**, 57–69.

114 X. Zhang, I. Belharouak, L. Li, Y. Lei, J. W. Elam, A. Nie, X. Chen, R. S. Yassar and R. L. Axelbaum, *Adv. Energy Mater.*, 2013, **3**, 1299–1307.

115 B. Xiao, B. Wang, J. Liu, K. Kaliyappan, Q. Sun, Y. Liu, G. Dadheech, M. P. Balogh, L. Yang and T.-K. Sham, *Nano Energy*, 2017, **34**, 120–130.

116 R. L. Patel, H. Xie, J. Park, H. Y. Asl, A. Choudhury and X. Liang, *Adv. Mater. Interfaces*, 2015, **2**, 1500046.

117 S. Sarkar, R. L. Patel, X. Liang and J. Park, *ACS Appl. Mater. Interfaces*, 2017, **9**, 30599–30607.

118 Y. Gao, R. L. Patel, K. Y. Shen, X. Wang, R. L. Axelbaum and X. Liang, *ACS Omega*, 2018, **3**, 906–916.

119 D. H. K. Jackson, M. R. Laskar, S. Fang, S. Xu, R. G. Ellis, X. Li, M. Dreibelbis, S. E. Babcock, M. K. Mahanthappa, D. Morgan, R. J. Hamers and T. F. Kuech, *J. Vac. Sci. Technol., A*, 2016, **34**, 031503.

120 K. Kaliyappan, J. Liu, A. Lushington, R. Li and X. Sun, *ChemSusChem*, 2015, **8**, 2537–2543.

121 L. N. Zhao, G. R. Chen, Y. H. Weng, T. T. Yan, L. Y. Shi, Z. X. An and D. S. Zhang, *Chem. Eng. J.*, 2020, **401**, 10.

122 Y. Gong, D. Palacio, X. Song, R. L. Patel, X. Liang, X. Zhao, J. B. Goodenough and K. Huang, *Nano Lett.*, 2013, **13**, 4340–4345.

123 R. L. Patel, Y. B. Jiang, A. Choudhury and X. Liang, *Sci. Rep.*, 2016, **6**, 25293.

124 B. Xiao, H. Liu, J. Liu, Q. Sun, B. Wang, K. Kaliyappan, Y. Zhao, M. N. Banis, Y. Liu, R. Li, T. K. Sham, G. A. Botton, M. Cai and X. Sun, *Adv. Mater.*, 2017, **29**, 1703764.

125 W. Lu, L. W. Liang, X. Sun, X. F. Sun, C. Wu, L. R. Hou, J. F. Sun and C. Z. Yuan, *Nanomaterials*, 2017, **7**, 325.

126 D. N. Wang, J. L. Yang, J. Liu, X. F. Li, R. Y. Li, M. Cai, T. K. Sham and X. L. Sun, *J. Mater. Chem. A*, 2014, **2**, 2306–2312.

127 E. Kang, Y. S. Jung, A. S. Cavanagh, G.-H. Kim, S. M. George, A. C. Dillon, J. K. Kim and J. Lee, *Adv. Funct. Mater.*, 2011, **21**, 2430–2438.

128 H. Sopha, G. D. Salian, R. Zazpe, J. Prikryl, L. Hromadko, T. Djenizian and J. M. Macak, *ACS Omega*, 2017, **2**, 2749–2756.

129 W. F. Mao, W. Yue, Z. J. Xu, J. Wang, J. B. Zhang, D. J. Li, B. Zhang, S. H. Yang, K. H. Dai, G. Liu and G. Ai, *ACS Appl. Mater. Interfaces*, 2020, **12**, 39282–39292.

130 A. Kohandehghan, P. Kalisvaart, K. Cui, M. Kupsta, E. Memarzadeh and D. Mitlin, *J. Mater. Chem. A*, 2013, **1**, 12850–12861.

131 E. M. Lotfabad, P. Kalisvaart, A. Kohandehghan, K. Cui, M. Kupsta, B. Farbod and D. Mitlin, *J. Mater. Chem. A*, 2014, **2**, 2504–2516.

132 Y. L. Li, L. C. Ma, Y. Yoo, G. C. Wang, X. D. Zhang and M. J. Ko, *J. Ind. Eng. Chem.*, 2019, **73**, 351–356.

133 S. Bose, T. Kuila, A. K. Mishra, R. Rajasekar, N. H. Kim and J. H. Lee, *J. Mater. Chem.*, 2012, **22**, 767–784.

134 J. Liu, M. N. Banis, Q. Sun, A. Lushington, R. Y. Li, T. K. Sham and X. L. Sun, *Adv. Mater.*, 2014, **26**, 6472–6477.

135 S. Y. Zhu, P. H. Xu, J. Q. Liu and J. M. Sun, *Electrochim. Acta*, 2020, **331**, 135268.

136 G. Wan, L. Yang, S. Shi, Y. Tang, X. Xu and G. Wang, *Chem. Commun.*, 2019, **55**, 517–520.

137 X. F. Li, X. B. Meng, J. Liu, D. S. Geng, Y. Zhang, M. N. Banis, Y. L. Li, J. L. Yang, R. Y. Li, X. L. Sun, M. Cai and M. W. Verbrugge, *Adv. Funct. Mater.*, 2012, **22**, 1647–1654.

138 Y. Zhong, X. H. Xia, J. Y. Zhan, Y. D. Wang, X. L. Wang and J. P. Tu, *J. Mater. Chem. A*, 2016, **4**, 18717–18722.

139 W. Xiong, Q. Guo, Z. Guo, H. Li, R. Zhao, Q. Chen, Z. W. Liu and X. W. Wang, *J. Mater. Chem. A*, 2018, **6**, 4297–4304.

140 X. B. Meng, Y. Q. Cao, J. A. Libera and J. W. Elam, *Chem. Mater.*, 2017, **29**, 9043–9052.

141 W. J. Lee, S. Bera, C. M. Kim, E. K. Koh, W. P. Hong, S. J. Oh, E. Cho and S. H. Kwon, *NPG Asia Mater.*, 2020, **12**, 13.

142 W. W. McNeary, S. F. Zaccarine, A. Lai, A. E. Linico, S. Pylypenko and A. W. Weimer, *Appl. Catal., B*, 2019, **254**, 587–593.

143 L. Zhang, Y. Zhao, M. N. Banis, K. Adair, Z. X. Song, L. J. Yang, M. Markiewicz, J. J. Li, S. Z. Wang, R. Y. Li, S. Y. Ye and X. L. Sun, *Nano Energy*, 2019, **60**, 111–118.

144 Y. F. Liu, L. X. Li, Y. Y. Wang and C. F. Li, *J. Inorg. Mater.*, 2017, **32**, 751–757.

145 G. Z. Wang, Z. Gao, G. P. Wan, S. W. Lin, P. Yang and Y. Qin, *Nano Res.*, 2014, **7**, 704–716.

146 G. Wang, X. Peng, L. Yu, G. Wan, S. Lin and Y. Qin, *J. Mater. Chem. A*, 2015, **3**, 2734–2740.

147 S. C. Zhao, L. L. Yan, X. D. Tian, Y. Q. Liu, C. Q. Chen, Y. Q. Li, J. K. Zhang, Y. Song and Y. Qin, *Nano Res.*, 2018, **11**, 530–541.

148 S. A. Skoog, J. W. Elam and R. J. Narayan, *Int. Mater. Rev.*, 2013, **58**, 113–129.

149 T. O. Kaariainen, M. Kemell, M. Vehkamaki, M. L. Kaariainen, A. Correia, H. A. Santos, L. M. Bimbo, J. Hirvonen, P. Hoppu, S. M. George, D. C. Cameron, M. Ritala and M. Leskela, *Int. J. Pharm.*, 2017, **525**, 160–174.

150 J. Hellrup, M. Rooth, A. Johansson and D. Mahlin, *Int. J. Pharm.*, 2017, **529**, 116–122.

151 M. J. Haghshenas-Lari, N. Mostoufi and R. Sotudeh-Gharebagh, *Part. Sci. Technol.*, 2017, **36**, 727–733.

152 R. L. Garcea, N. M. Meinerz, M. Dong, H. Funke, S. Ghazvini and T. W. Randolph, *npj Vaccines*, 2020, **5**, 45.

153 D. Zhang, M. J. Quayle, G. Petersson, J. R. van Ommen and S. Folestad, *Nanoscale*, 2017, **9**, 11410–11417.

154 J. Hellrup, M. Rooth, E. Martensson, K. Sigfridsson and A. Johansson, *Eur. J. Pharm. Biopharm.*, 2019, **140**, 60–66.